Multi length scale porosity as a playground for organic thermoelectric applications

Quentin Weinbach, Christian Nielsen, Laure Biniek

Multi length scale porosity as a playground for organic thermoelectric applications

Authors: Quentin Weinbach, Christian B. Nielsen, Laure Biniek*

Q. Weinbach, Dr. L. Biniek (ORCID: 0000-0002-7643-3713)

Université de Strasbourg, CNRS, Institut Charles Sadron UPR22, F-67000 Strasbourg, France

*Email: laure.biniek@ics-cnrs.unistra.fr

Dr. C. B. Nielsen (ORCID: 0000-0002-8591-1203)

Department of Chemistry, Queen Mary University of London, Mile End Road, London E1 4NS, United Kingdom

Short Bio

Quentin Weinbach is a Ph.D student at Institut Charles Sadron in Strasbourg. He received his M.S degree in material engineering and nanosciences from the University of Strasbourg and his engineering degree in functional materials and nanosciences from the European School of Chemistry, Polymers and Materials in Strasbourg in 2019. His research focuses on porous polymer thermoelectric materials.

Christian Nielsen received his Ph.D from the University of Copenhagen in Denmark in 2004. His main research focus is centered on the design and synthesis of new semiconducting materials for organic electronic applications.

Laure Biniek is a CNRS researcher at Institut Charles Sadron in France. She received her Ph.D degree from Strasbourg University in 2010. Her research interests focus on structure-property correlations in semi-conducting polymers for organic electronics. She is currently developing porous conducting polymers for thermoelectrics.

Abstract

Porous organic materials have interesting materials properties governed not only by their covalent structure but also by their intrinsic porosity which when controlled over multiple length scales gives rise to micro-, meso- and macroporous materials. These materials have been exploited for many years in applications such as gas storage, filtration/separation membranes, or support for catalysts. More recently, porous materials have attracted significant attention as potential harvesters of the abundant waste heat generated in today's society. Taking advantage of the thermoelectric effect, whereupon a temperature gradient is converted to electric voltage, thermoelectric materials and their associated applications are well-suited for this endeavor. Efficient thermoelectric material must combine a high electrical conductivity and a low thermal conductivity. Since in porous materials, these properties can potentially be optimized independently, they are intriguing candidates for further exploration. Here, we give an overview of

the different classes of porous conducting polymers (PCPs) and provide a thorough survey of their recent use in the broader context of thermoelectrics. We also aim to identify the major challenges and future perspectives for porous organic thermoelectric materials.

A. Introduction

Much research has been devoted to the development of high-performance energy conversion and storage systems based on conducting polymers (CPs). The advantages of such organic materials compared to the inorganic conductors include their ease of molecular tailoring, conformability and flexibility, ease of processing, light weight and potentially reduced cost. To meet the challenges of high-performance energy conversion devices (often strongly dependent on charge transport properties), the development of new materials and the judicious control of their structure are of particular importance. In recent decades, conducting polymer (thin and thick) films have constituted the main points of attention, but rapid advancement in nanoscale science has also promoted the development of 1D systems (such as nanowires) from controlled nanostructured CPs. Naturally, it is anticipated that CPs with well-defined nanostructures can maintain the properties to their bulk forms while simultaneously exhibiting unusual chemical/physical properties because of the confined dimensions of the nanomaterials. The concept of assembling nanostructures into macroscopic 3D polymer architectures previously developed for applications such as separating membranes,[1] thermal insulators,[2] or support for catalysis,[3,4] has consequently begun to attract attention over recent years in the context of energy conversion. While it is anticipated that the electronic properties of CPs can be maintained or even enhanced when going from 1D and 2D systems to macroscopic 3D architectures through careful molecular design, the 3D structure introduces the concept of free volume or porosity as a potentially beneficial property that can likewise be controlled through rational design and synthesis.

Thus, porous 3D architectures based on conjugated polymers have recently emerged as a new class of conducting materials for a range of organic electronic applications. Their extended π-conjugated properties due to their 3D network make them very interesting candidates in applications such as ultralight supercapacitors,[5–12] batteries,[13–16] wearable energy storage devices,[9,10,17] biomedical applications[18–20] and energy conversion.[10,17,21–27,28–32] The energy harvesting applications such as organic photovoltaics and thermoelectrics rely on the close interaction of two or more components such as electron donor and acceptor in photovoltaics and organic polymer and molecular dopant in thermoelectrics. With this in mind, **porous conducting polymers** (**PCPs**) offer an interesting avenue for modifying and controlling the chemical and physical environment of the inherent free volume. This will be advantageous for controlling the interplay between the porous framework material and the second "guest" entity such as a molecular dopant. Furthermore, introducing porosity into semi-conducting materials is considered as a smart strategy for tuning down their thermal conductivity and thus inversely improving thermoelectric (TE) efficiency.

Given the constraints imposed by the TE applications, PCP material design rules are still in need of clarification before reaching "ideal" porous structures.

In this review, we aim to summarize the recent developments on the use of porous architectures based on π-conjugated polymers as a playground for challenging organic electronic applications with a particular focus on organic thermoelectric devices. The approach is original in that we look at the structure – property relationship of different subclasses of PCPs, i.e. covalent organic frameworks (COFs), conjugated microporous polymers (CMPs), and dried gels, focusing on electronic and thermoelectric properties. Only porous materials for which the porous matrix is conductive will be discussed.

B. A brief introduction to the different classes of porous conducting polymers

There are many different classes of porous conducting materials based on conjugated polymer. Regrettably, the terminology used across the vast literature is ambiguous and non-consistent. Some authors describe polymer gels as conjugated microporous polymers (CMPs).[5–7,13,33] Others define those same conjugated microporous polymers as polymers of intrinsic microporosity (PIMs). Furthermore, polymers with pores in the micrometer scale are sometimes called microporous polymers whereas they should be classified as macroporous polymers according to the IUPAC recommendation. In this review, we will briefly introduce the different classes of materials and their IUPAC recommended nomenclature[34] to clarify the often confusing descriptions of porous polymer.

The first criterion is the size of the pores. Polymeric material with pore sizes not exceeding 2 nm should be classified as microporous polymers. Mesoporous polymers have intermediate pore sizes in the range of 2-50 nm. Macroporous polymers have pore sizes larger than 50 nm (see Figure 1). Within those classes of porous polymers, four main types of PCPs, presented below, have been used for organic electronic applications.[35]

In order to maintain inner cavities, rigid polymer networks must be built up to prevent collapse of polymer chains into a nonporous dense state. One of the key strategies for this purpose is the use of rigid building units (conjugated units) fixed either with strong covalent bonds (for microporous polymers) or with coordination bond (for covalent organic framework). Another strategy is to form coherent network of connected polymer objects (fibers/ aggregates/colloids/…) through a liquid-solid phase transition, providing after solvent evaporation, dried gels.

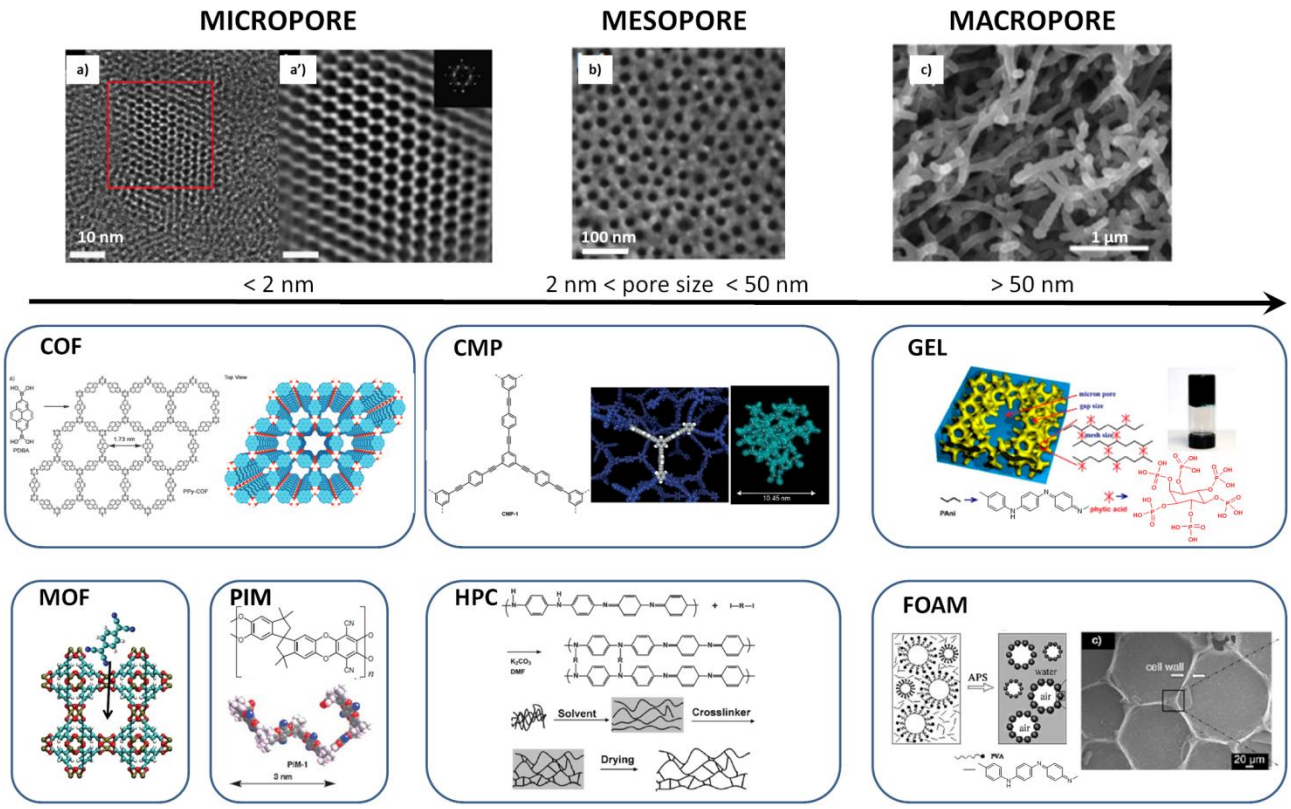

Figure 1: Illustration of the diverse range of pore sizes that can be found in PCPs: a-a') High Resolution and Fourier-filtered images of COF1, respectively (reproduced with permission from Nat. Comm.[36]) ; b) SEM image of 2D Graphene Oxide based mesoporous polypyrrole nanosheets (reproduced with permission from Nat. Comm[37]) ; c) SEM image of nanostructured polypyrrole hydrogel with CuPcTs as dopant (reproduced with permission from Nano Lett[38]); and illustrations of the structure of different types of porous materials such as covalent organic framework (COF)[39] ; conjugated microporous polymer (CMP)[40] ; gel[41]; metal-organic framework (MOF)[42] ; polymer of intrinsic microporosity (PIM)[1] ; hypercrosslinked polymer (HPC)[43] ; and foam[44]. All panels have been reproduced with permission from Angewandte Chemie, (COF and CMP), PNAS (gel), Science (MOF), The Royal Society of Chemistry (PIM and HPC), and ChemPhysChem (foam).

B.1. Covalent Organic Framework (COF)

Covalent organic frameworks (COFs) are purely organic coordination polymers with an open framework extending in two or three dimensions. COFs are synthesized using dynamic covalent chemistry, taking advantage of reversible bond formations. This built-in thermodynamic control allows a so-called error-checking during the synthesis. Due to the richness of the organic chemistry toolbox, an endless number of vertices and linkers can be used to construct a plethora of frameworks with different pore shapes (hexagonal, tetragonal, rhombic, and trigonal) and

different pore sizes (typically 1-5 nm) as illustrated for a hexagonal structure in Figure 1 (left hand side image). Unlike the other PCPs described hereafter, this synthesis strategy allows a rational pore size engineering at a molecular level and a fine-tuned control over the topology of the structure, providing crystalline frameworks. Bulk COF synthesis produces insoluble powders that are difficult to process due to the highly crystalline nature of the framework. However, different synthetic protocols such as liquid-liquid interface synthesis and solvent-mediated exfoliation are being developed,[45–47] which provide means for thin film formation and a better control of the microstructure over different length scales. COFs are emerging as an important class of porous organic materials with interesting and tunable properties for a variety of applications such as gas separation and catalysis.[45] Semiconducting COFs have been reported as early as 2008, but the implementation into organic electronic devices is still in its infancy.[48,49]

COFs should be confused neither with metal organic frameworks (MOFs) nor conjugated microporous polymers (see section 2.2.), the porous structure of which also fall within the micropore size range (see Figure 1). MOFs are inorganic–organic hybrid materials comprised of single metal ions or polynuclear metal clusters linked by organic ligands principally through coordination bonds. Due to the strength of these coordination bonds, MOFs are geometrically and crystallographically well-defined framework structures. MOFs are also known as porous coordination polymers. Since however they are mostly based on metals, they will not be considered in this review.

B.2. Conjugated microporous polymers (CMPs), polymers of intrinsic microporosity (PIMs) and hypercrosslinked polymers (HCPs)

Unlike COFs, which are synthesized under thermodynamic control, 3D networks of **conjugated microporous polymers** (CMPs) are formed by irreversible covalent bonds and the polymerization proceeds via a kinetic route. Consequently, nearly all CMPs are amorphous (there are a few exceptions). CMP networks can be formed through the reaction of two or more different monomers or, in some cases, by homocoupling of a single monomer. Extended π-conjugated microporous networks are obtained when conjugated units are linked together, either directly, or via double or triple bonds through C-C cross coupling reactions.[50] The development of CMPs started in 2007 with the synthesis of poly(aryleneethylene) network.[40] Since then, the field of CMPs materials has grown considerably, given their wide range of potential applications exploiting both the optoelectronic properties and the presence of permanent voids within their structure. As for COFs, the pore structure can be tuned by varying the monomer geometry and length or by the use of co-monomers. Their average pore diameter is generally less than 2-5 nm.

The most common approach to synthesize CMPs is the combination of a conjugated core of C3 symmetry (e.g. 1,3,5-triethynylbenzene) with a linker with C2 symmetry (e.g. 1,4-diiodobenzene, as illustrated in Figure 1).

Depending on their synthesis routes or their chemical structures, other sub-classes of CMPs have been reported. For the potential purpose of TE application, we will briefly describe hypercrosslinked polymers (HPCs) and polymers of intrinsic microporosity (PIMs).

Hyper-crosslinking of preformed linear conjugated polymers such as polyaniline or polypyrrole provides another approach to produce CMPs. They are known as **hypercrosslinked polymers** (HCPs) (see Figure 1). The reaction method, choice of solvent, and choice of cross-linker greatly affected the porosity.[50] However a high number of crosslinking bonds limit the solubility and processability of HPCs. From a synthetic perspective, HCPs are predominantly prepared by the following three approaches: (1) post-crosslinking polymer precursors, (2) direct one-step

polycondensation of functional monomers, and (3) knitting rigid aromatic building blocks with external crosslinkers.

Polymers of intrinsic microporosity (PIMs) refer to a specific class of rigid chain-contorted microporous polymers (ladder-like structure). Intrinsic microporosity is defined as a continuous network of intermolecular microcavities of less than 2 nm, which is formed as a consequence of the inefficient packing of the rigid and twisted polymer backbone (see Figure 1). The contortion site (often a tetrahedral carbon atom) causes the polymer to fill the space ineffectively. In the archetypal soluble PIM1, a spirobisindane function acts as a center of contortion (Figure 1). When the solvent is removed, the free volume between polymer chains leads to an open pore structure.

B.3. Conducting gels

Gels constitute a vast class of materials that can be subdivided into two categories: chemical gels and physical gels, the latter being also referred as thermo-reversible gels if the regions of local order are thermally reversible. According to IUPAC, gels are defined as non-fluid colloidal networks or polymer networks that are expanded throughout their whole volume by a fluid. The networks are composed of connected objects. For the chemical gels, the connectedness is achieved by covalent bonds (via crosslinking or non-linear polymerization). For physical gels, the co-operative bonds are less energetic (e.g. Hydrogen-bonds or van der Waals interactions).[51]

According to those definitions, we will consider the so-called “crosslinked polymer network” or “crosslinked conductive polymer gels”[41] as chemical gels. As an example, the research works of L. Pan,[41] Y. Shi[52] and co-workers illustrate well a dopant crosslinking method to synthesize conductive polyaniline hydrogels. Multifunctional dopant molecules such as phytic acid or copper

phthalocyanine-3,4',4",4"'-tetrasulfonic acid tetrasodium salt (CuPcTs) interact with more than one polymer chain (by protonation) to form an interconnected porous network (see Figure 1). Another method to produce chemical gels consists in in-situ polymerization of the conductive gel precursors through chemical oxidation coupling. PEDOT (poly(3,4-ethylenedioxythiophene)), polypyrrole or polyaniline hydrogels can be synthesized with the presence of a series of oxidant such as $FeCl_3$, $Fe(NO_3)_3$ or $(NH_4)S_2O_8$ with a controlled oxidation rate.[53] In both dopant crosslinking and in-situ polymerization methods, the coherent network formed during the gel formation influences strongly the final microstructure.

In contrast to chemical gels, the polymer physical gel network can be formed through the physical aggregation of polymer chains (caused by hydrogen bonds, crystallization or complexation) or through glassy junction points. Some gel structures can also be formed via lamellar mesophases.[53] Polymer physical gels are mostly formed by cooling a mixture of miscible components (i.e. polymer and solvent). The polymer undergoes a liquid-solid transition below a so-called gelation threshold while the solvent remains liquid. The polymer chains create therefore a framework within which the solvent is confined. In the case of water, such structures are called hydrogels. (Reminder: organogels are made by small molecule gelators and not polymer gels in organic solvent).[54,55]

Physical gels can be used as such or dried by removing the solvent. Several techniques have been developed.[56] Depending on the drying method, the polymer dried gels are named xerogels (ambient in air drying), aerogels (supercritical drying), or cryogels (freeze drying), (see Figure 2). It is clear that the drying process is a key step as it plays a major role in the final internal structure of the porous network. For instance, the polymer network may collapse during drying because of capillary stress changes through the direct liquid –gas transition (case of xerogels). To avoid this 'fatal' issue, it is preferred to go through the solid-gas barrier (removing the solvent by freezing

followed by sublimation, case of freeze-drying) or to dry the gel beyond the critical point, at high temperature and pressure (supercritical drying).

Supercritical drying of gels is an interesting path because the liquid is transformed into gas in the absence of surface tension and capillary stress: it can guarantee conservation of the porous gel structure.[57] Importantly, the solvent of the gel must be fully miscible in liquid CO_2 (i.e. ethanol, acetone). The solvent/liquid CO_2 blend is brought to a sufficiently high temperature and pressure (typically, above 31°C and 7.5 MPa which corresponds to the critical point of pure CO_2) to reach its supercritical state before being replaced by pure supercritical CO_2. At this point, the supercritical fluid continuously flows through the sample's pores by depressurizing the autoclave. Then, pressure is slowly released, until the supercritical CO_2 reverts to its gas form. In theory, at the critical point, the supercritical fluid loses all surface tension and can no longer exert capillary stress. However, for pressure/temperature sensitive samples such as polymer gels, supercritical drying parameters have to be finely controlled to avoid any shrinkage.

Conversely, freeze drying technique is easier and less aggressive for sensitive samples. The gel is firstly frozen (with liquid N_2) to prevent structure collapsing, then the solvent is removed by sublimation of the crystals (ice in the case of hydrogels) providing cryogels. This technique allows preparing robust cryogels but the pore size is determined by the size of ice crystals. At the end, dried 3D architectures are extremely porous: up to 99.8% of their volume is air.[53] The mechanical properties of the dried gels should be fairly similar to those of the thermoreversible gels.

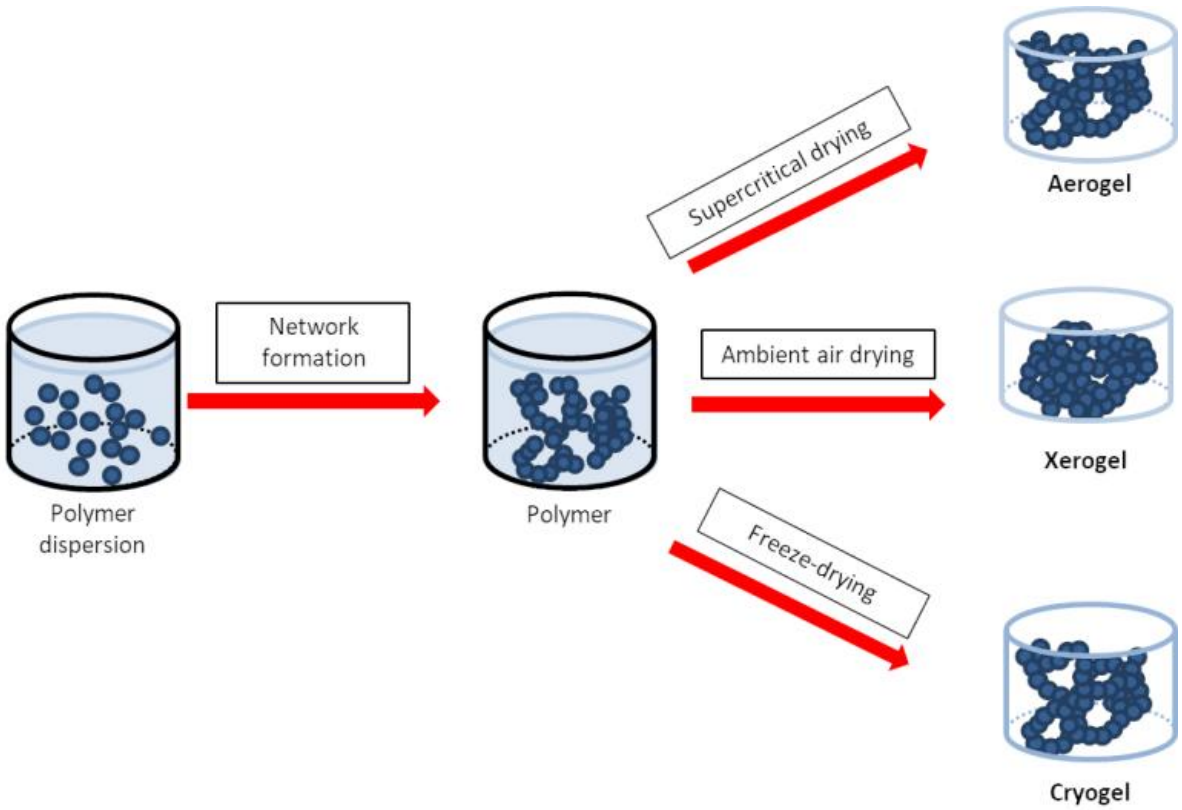

Figure 2: Schematic routes to fabricate polymer gel network and dried gels, case of PEDOT:PSS. The polymer chains are represented by the dark blue beads while the solvent (water) is in light blue.

B.4. Conducting polymer foams

Even though many porous gels have pore geometries which resemble those of polymer foams, they commonly form two separate sub-classes in the wider class of macro-porous polymers. This separation is given by the method of production combined with the physical mechanisms which control the pore geometries. Unlike porous gels, polymer foams are obtained by creating closely packed gas bubbles in an initially liquid or visco-elastic medium which is then solidified through polymerization/cross-linking/drying. These gas bubbles can be created by many different means (physical or chemical blowing, mechanical agitation, etc.). They are commonly (but not necessarily) larger than 10 micrometers and separated by thin pore walls of characteristic thicknesses of 0.1-1 micrometer in "closed-cell foams". These pore walls can break during the solidification stage, leading to "open-cell foams" (or sponges). In either case, the recognizable

characteristic pore shapes of the resulting polymer foam are controlled by the mechanical stresses arising from the minimization of the interfacial energies of the gas/liquid interfaces in the liquid state. To the best of our knowledge, only a few pure organic conducting polymer-based foams have been obtained, all of them being composites. An example of PANI/PVA foams and their porous structure is given in Figure 1. Heng and coworkers[44] proposed that PVA foams firstly formed by mechanical frothing and are then enwrapped by PANI molecules. Their uses in optoelectronic applications are limited by the foam stability (drainage or creaming effect leading to a heterogeneous porous structure) and the low mechanical properties of the dried films.

C. Porous conducting polymers for thermoelectric applications

C.1. Introduction to organic thermoelectrics

Now, let us discuss the potential of **PCPs** for organic thermoelectric applications. Around two thirds of our primary energy resources are currently wasted as heat due to inefficient energy conversion processes, making waste heat harvesting an important focus point in the world's drive to net zero carbon emission. Although dominated by inorganic thermoelectric generators, organic thermoelectric materials hold great promise for low-grade waste heat harvesting at relatively low temperatures where inorganics suffer from poor efficiencies.

The suitability of any thermoelectric material is evaluated by its dimensionless figure of merit *ZT*, expressed by:

$$\mathrm{ZT} = \frac{\sigma.\mathrm{S}^2}{\mathrm{k}}\mathrm{T} \quad \text{(eq. 1)}$$

Where σ, S, κ and T are electrical conductivity, Seebeck coefficient, thermal conductivity, and absolute temperature, respectively. Thus, to reach high *ZT*, the thermoelectric material must

combine metal-like electrical conductivity and Seebeck coefficient while being thermally insulating.

For now, the best thermoelectric materials are inorganic telluride and tin selenide-based alloys (with $ZT > 2$).[58–61] Such materials are rare, expensive and highly toxic. Conversely, conducting polymers that are less expensive and more environmentally friendly have become a recent source of interest to the scientific community. In particular, a major attraction is their very low thermal conductivity compared to the inorganic compounds. However, the overall efficiency of polymer conductors ($ZT = 10^{-3} – 10^{-1}$) is limited by their low Seebeck coefficient.[62–64] On a general basis, polymer TE is an emerging field that has only developed since the pioneering work of Bubnova and co-workers in 2011.[65] Since then, a large body of work has been produced with the aim of improving doping efficiency,[66–68] controlling in-plane morphology and crystallinity[69–71] or enhancing the Seebeck coefficient by blending polymers with varying broadness of density of states (DOS).[72,73] As major breakthroughs, one can note the improvement of the power factor ($PF = S^2\sigma$) and a better understanding of the interplay between S and σ.[67,74] As an example, Vijayakumar and coworkers show that a combination of in-plane alignment and a doping protocol of the polymers maintaining a percolating nanomorphology along the chain direction lead to record power factors of 2 mW m^{-1} K^{-2}.[75] However, in such highly doped samples, the thermal conductivity could be highly dominated by a high electronic contribution, dramatically increasing κ and thus limiting ZT.

Let us emphasize however, again, that this “outlook” does not aim at offering a complete survey of all the research in this field. Comprehensive and more complete reviews on recent progress in organic TE can be found in the literature.[64,76–79]

C.2. Why is porosity of interest for thermoelectric applications? How should thermoelectric performances in porous structure be measured?

The use of porous bulk conductive soft materials is particularly appealing for both the possible tailoring of thermal conductivity and the integration into a thermoelectric generator reliant upon large scale accessible surface area. Thermoelectricity depends mainly on a temperature difference between two complementary materials which results in energy production (see Figure 3). Such control of a temperature difference is rather difficult with nanometer sized samples (thin films). That is why *bulk sized* organic thermoelectric materials are needed in order to create thermoelectric generator prototypes.

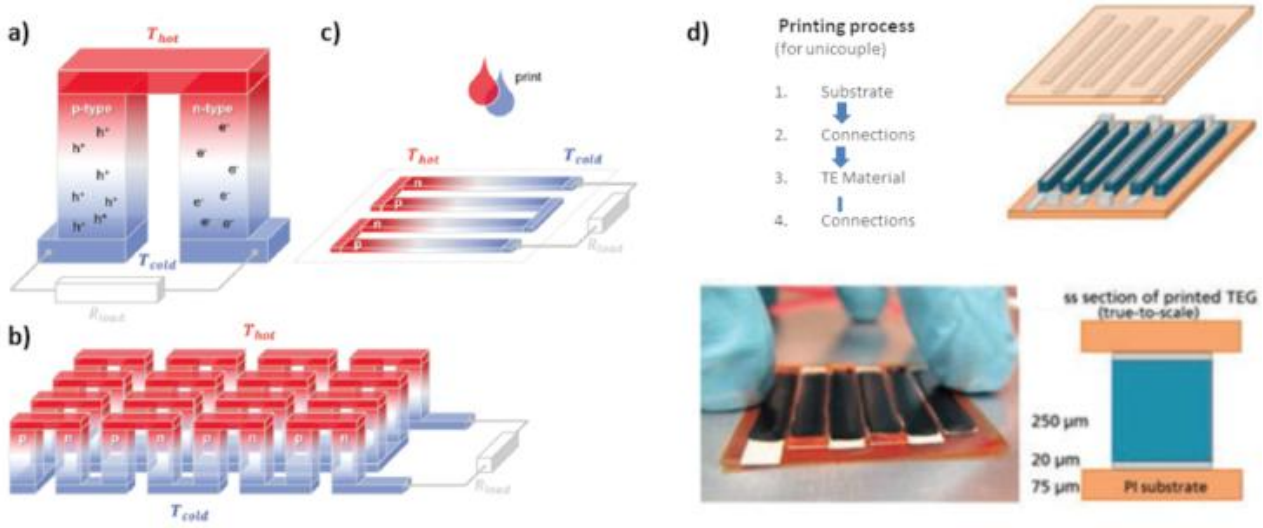

Figure 3: Schematics of (a) a thermoelectric element, which comprises one n- and one p-type thermoelectric leg that experience a temperature gradient $\Delta T = T_{hot} - T_{cold}$ leading to charge accumulation at the cold ends, (b) a conventional thermoelectric module that comprises an array of elements, which are connected electrically in series but thermally in parallel, and (c) an in-plane (printable) array of elements. generators (according to ref.[77] reproduced with permission from the Royal Society of Chemistry). From the perspective of applications, thermoelectric generators (TEGs) containing a large number of thermoelectric p- and n-type legs connected in series are needed to achieve considerable power output. Bulk PCPs are compatible with vertical device geometry. d) From the perspective of evaluating the performances of a material, connecting in series vertical mono leg TEG (only one type of polymer) can be easily produced. In this case, a conductive electrode (gold or silver paste) is replacing the second type of leg. The printing sequence, scheme of a

vertical TEG design and image of a vertical PEDOT:PSS TEG printed with a dispenser is shown as a proof of concept.[80]

Furthermore, inspired by the highly performant silicon aerogels,[81] nanostructured polymer aerogels[2] make excellent candidates as best thermally insulating materials (κ < 0.03 W m^{-1} K^{-1}) with unique characteristics, such as fine internal void spaces, open-pore geometry and trapped air in the meso-/ micro-porous structure. Using conducting polymers to make such porous 3D architectures is therefore of interest to reach low κ while maintaining a reasonably high power factor for TE application.

To take the most benefit out of PCPs, one needs to understand the breakthroughs related to the thermal conductivity.

For a macroporous structure (with pore size >> 70nm, the value of mean free path of air), the simplest approach consists in considering a two-phase mixture model: the solid phase and the gas phase weighted by their respective volume fraction.[82] As an example Kroon et al.[28] applied the rule of mixtures to predict the thermal conductivity of their "doped P3HT foam" (κ_{porous}) following the equation:

$$\kappa_{porous} = \kappa_{solid}\left(1 - \frac{p}{100}\right) + \kappa_{air}\frac{p}{100} \qquad \text{(eq. 2)}$$

Where κ_{air} (= 0.025 W m^{-1} K^{-1}) and κ_{solid} and p are the thermal conductivity of air, solid polymer and the porosity, respectively. The decrease in thermal conductivity in the foam sample (0.14 W m^{-1} K^{-1}, measured by the transient plane source method) as compared with the solid doped P3HT (0.32 W m^{-1} K^{-1}) is mainly attributed to the low density of the foam (which contains 66% of air in a mm-thick PCP sample).

For a meso-/ micro-porous structure, one needs to consider more complex heat transport mechanisms in porous media.

Heat transfer through an electrically insulating porous medium is carried by phonons. It has been conventionally considered as a combination of thermal conduction along its solid matrix (κ_s), thermal radiation across internal pores (κ_{rad}), and either thermal convection (κ_{conv}) by or conduction through gases (κ_g) filling the pores. Thus, the total thermal conductivity ($\kappa_{lattice}$) of an electrically insulating medium is calculated by:[83]

$$\kappa_{lattice} = \kappa_s + \kappa_g + \kappa_{rad} + \kappa_{conv} \quad \text{(eq. 3)}$$

Convective heat transfer requires that gas is transported across the full temperature gradient within the material. In bulk (thick) materials, the contribution from convection can be disregarded when the pore sizes are sufficiently small (<1 mm). The radiative thermal conductivity rises with an increase in pore size and most importantly shows a power law temperature dependence (T^3).[84] Therefore, at ambient temperature and pressure conditions, the radiation contribution is also negligible. The two last components (gas and solid thermal conductivities) are highly dependent on the porous structure.

The gas thermal conductivity can be described as follow:

$$\kappa_g = \frac{\kappa_g^0}{1+2\beta Kn} \quad \text{(eq. 4)}$$

$$Kn = \frac{\Lambda_g}{D} \quad \text{(eq. 5)}$$

Where κ_g^0 is the thermal conductivity of the gas in free space, β is a coefficient depending on accommodation and adiabatic coefficients of the gas (typically β = 2 for air)[85] and Kn is the Knudsen number defined as the ratio between the mean free path of the gas molecules Λ_g (typically 70 nm for air at ambient pressure and temperature conditions) and the mean pore diameter D.[2,86] Thus, in order to minimize the gas thermal conductivity, below the one of air (25 mW m^{-1} K^{-1}), one must reduce the size of the pore below 70 nm. When the pore diameter is inferior to the mean free path of air (e.g. Kn > 1), the transport mode of the gas molecule is known

as Knudsen diffusion.[87] In this regime, the molecule-wall interactions dominate over molecule-molecule interactions conversely with normal diffusion. This effect can drastically reduce the gaseous thermal conductivity component that can consequently be neglected in the calculation of the total thermal conductivity.

(Note: gas-solid coupling effects can also have a significant impact on heat transfer and contribute to the total thermal conductivity. The coupling component depends on the solid phase structure and the pore size.[88] The theoretical models are mostly based on the assumption of spherical particles in the solid backbone which cannot fit with the structure of PCPs. Too little is known at the moment to consider the contribution of this coupling effect, although it should not be ignored.)

Finally, the solid thermal conductivity (κ_s) can be calculated by Eq. (6):

$$\kappa_s = \kappa_0 \frac{\rho v}{\rho_0 v_0} \qquad \text{(eq. 6)}$$

where κ_0 is the thermal conductivity of the solid backbone, ρ and ρ_0 are respectively the density of the bulk porous material and of the solid backbone, v and v_0, respectively the sound velocity in the bulk porous material and in the solid backbone. According to the kinetic theory, κ_0, in its simplest form, is given by the Debye formula:

$$\kappa_0 = \frac{1}{3} C_v v \Lambda_{phonons} \quad \text{(eq. 7)}$$

where C_v is the lattice specific heat at constant volume, v is the group velocity of phonons (the velocity of sound) and $\Lambda_{phonons}$ the phonon mean free path. As seen from Equations 6 and 7, the solid contribution to the thermal conductivity can be reduced by minimizing the density of the bulk porous material and the phonon transport. A low bulk density is necessary to maintain a low solid thermal conductivity.[89] The propagations of phonons on the polymer chains can be hindered by scattering events such as those at boundaries (chain ends), interfaces (amorphous-crystalline

domain boundaries, pores), or between two adjacent chains (intermolecular scattering).[90] As such, micro-/ meso-porosity constitutes a major impediment for phonon transport as holes/pores can scatter phonons, in particular at solid-gas interfaces. The scattering and loss in energy is even greater if the pore dimension is of the order of magnitude of the mean free path of a phonon.

In the case of electrically conducting materials, one needs also to consider an electronic contribution (κ_{elec}) to the total thermal conductivity according to:

$$\kappa = \kappa_{elec} + \kappa_{lattice} \text{ (eq.8)}$$

The electronic contribution corresponds to the heat carried by the electrical charges when they delocalize and can be described, in general, by the Wiedemann-Franz law (WFL):

$$\kappa_{elec} = \sigma LT \qquad \text{(eq. 9)}$$

where *T* is the temperature in Kelvin, σ is the electrical conductivity in S m^{-1} and *L* is the Lorenz number. Since the electronic contribution κ_{elec} is proportional to σ, it cannot be tuned to optimize *ZT*. However, as discussed previously, decreasing the lattice contribution can be of interest to reach low total κ values independently of electrical conductivity. As a matter of fact, Scheuenemann et al[91] demonstrated that reaching ZT value beyond 1 with organic thermoelectrics would require to decrease $\kappa_{lattice}$ below 0.2 W m^{-1} K^{-1}.

To summarize, in order to obtain an useful reduction of the thermal conductivity of PCPs, one needs to focus on i) reducing its lattice contribution (low material density) and ii) reducing the pore size below the mean free path of air. Strategies aiming at decreasing the pore size to restrict the thermal conductivity are known as phonon engineering. This concept has been validated both theoretically and experimentally for MOF materials.[92] Because of the novelty aspect and the challenges of elaborating homogeneous and controlled structure, phonon engineering has not yet been reported in PCPs.

Let us now discuss the practical aspect of measuring thermal conductivity of organic materials, which is not straightforward. Many different experimental techniques can give access to the thermal properties of a material. They are distinguished according to the heat conduction conditions which are considered (i.e. at steady state or transient state). One can also use time domain or frequency domain methods such as the laser flash, transient plane source or 3ω-methods. However special attention should be paid when applying one or the other technique since the measurement accuracy and reliability are significantly affected by the sample characteristics (e.g. size, morphology, mechanical, thermal and optical properties). A suitable method should also be selected according to the temperature range of the measurements and the range of thermal conductivity of the materials. An excellent review by Wang et al. reports on the operating principles, merits and limitation of the different techniques available to measure the thermal conductivity of organic TE materials.[93] Only a few of them can be applied to PCP characterizations, the most popular for bulk porous samples being the transient plane source method. Because of the inherent experimental limitations and the lack of theoretical models on heat transport in porous conducting organic materials, the absolute values of thermal conductivity found in the literature for PCP must be taken with precaution. Crosschecking the results by different techniques is highly desirable for ensuring credibility.

Clearly, continuing experimental and theoretical developments on thermal conductivity characterization are highly needed to evaluate properly the efficiency of porous TE materials.

Charge transport properties of the PCPs, together with their thermal conductivity must be controlled for thermoelectric applications. High electrical conductivity requires high charge carrier mobility and/or density. In view of their relatively large band gap (1.5 to 3 eV), semi-conducting polymers need to be doped either chemically or electrochemically to become conductive. For organic molecules, the chemical doping process amounts to introduce organic dopant molecules

within the polymer matrix. The dopants will either donate electrons to or receive them from the polymer (for n- and p-type doping, respectively).[33,94] Of course, the introduction of dopants is likely to disrupt the structural order within the polymer matrix and negatively affect the charge carrier mobility.

Negative (electrons) and positive (holes) charge carriers migrate through the π-conjugated polymer chains (intra-chain) and by charge hopping from chain to chain (inter-chain). Charge transport in polymer semiconductors has been investigated for several decades and excellent reviews of this topic do exist.[95,96,97] Theoretical approaches have shown that charge transport is mainly driven by intra-chain transport, which is two to three orders of magnitude faster than inter-chain transport.[98,99] However, since the chain length of polymers is much shorter than the thickness of an active layer, to get from one electrode to the other through a polymer film, inter-chain hopping of electronic charges is mandatory. This hopping is related to the intermolecular interactions and therefore to the structural order within the polymer film. This order includes π-stacking interactions, nanoscale order of the polymer chains and polymer crystallinity.[100] Understanding the charge transport properties in organic TE is even more complicated since the charge carrier density (and not only the mobility) and the strong interplay between σ and S must be considered. Despite the use of different charge transport models that can be applied to semiconducting polymers (i.e. the mobility edge or the variable range hopping models, both pioneered by Mott)[101,102], the empirical power laws between the thermopower and the charge conductivity described by several groups are not yet fully understood.

In short, while remarkable efforts have been made to understand the charge transport behavior in organic TE bulk film, there is a critical lack of theoretical models in organic porous structures.

We can anticipate that electrical conductivity in porous bulk organic conductor materials is lower than in thin films: the pore formation induces separation between crystalline domains and structural/energetic disorder within these domains. A lower percolation is also expected in porous

structure. Indeed, as demonstrated for porous manganese oxide, both the large air content and the small size of pores are detrimental for electrical conductivity.[103]

Investigations on metallic foams have however revealed that geometrical factors of the porous structure (closed or open cells; pore volume fraction; pore size) play a major role on the electrical resistivity of the material.[104,105] Whether these models on relative conductivity/resistivity as a function of porous geometrical in metallic foams can be transferred to organic materials will be established only after further developments in PCPs.

The last issue, but not the least one, deals with the accuracy of the electrical conductivity measurements. The most common technique, the 4-probe resistivity method is relatively straightforward for homogeneous thin films. But, in theory, the method cannot apply to heterogeneous systems. Furthermore, for measurements on thick/bulky samples, geometrical factors with the probe arrangement come into play. Correction factors must be applied when the thickness of the sample is over twice the distance between the probes. For a comprehensive case study, we refer the reader to the work by Haldor Topsøe in 1966.[106] Regrettably, in most of the research works discussed below, we could not find the relevant experimental information that would have allowed us a more in-depth comparison. We invite the researchers working in this field, to share with the community, the measurement set-up characteristics, sample shape and thickness, and equation used to determine the charge conductivity out from the measured resistance value.

Similarly, because of the lack of experimental information on Seebeck coefficient measurements, we were only able to discuss the absolute values of *S* reported in the literature.

C.3. Which types of PCPs have been investigated in the context of thermoelectrics in the last 5 years?

In the following, we attempt a review of the different types of PCPs developed in the last five years for TE applications. We focus on how their porous structure and morphology can be controlled and how these parameters impact the properties. Special attention is paid to the main physical properties such as electrical conductivity (σ), porosity, density and thermoelectric properties. Table 1 summarizes the key parameters of the best performing materials. The review is organized as follows: microporous PCP structures are discussed first, whereas meso- and macro-porous structures are presented together.

C.3.1 Microporous structures

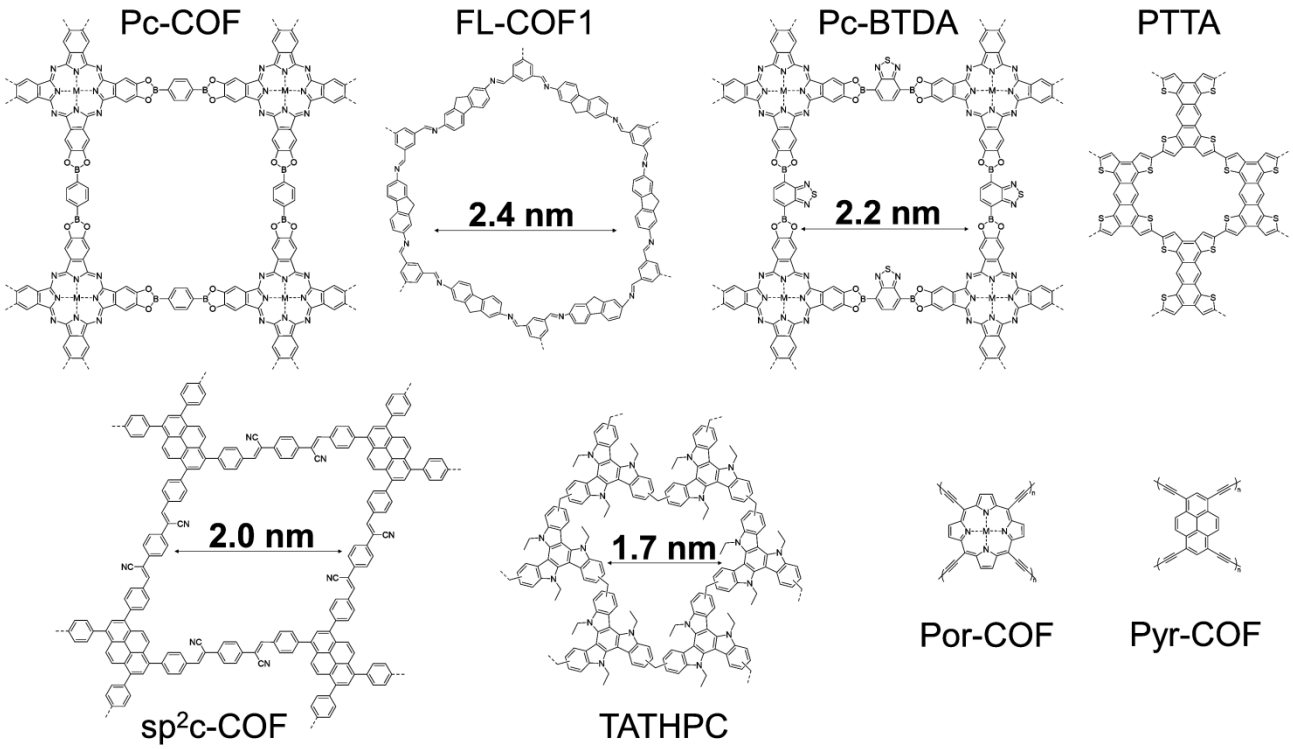

Figure 4: Chemical structure of COFs and HPC.

C.3.1.a. Microporous structures based on COFs

Much work has been devoted to the thermoelectric properties of metal-organic frameworks (MOFs), with reports of high electrical conductivities, low thermal conductivities and *ZT* values on the order of 10^{-3}.[92,107] By contrast, their purely organic counterparts, covalent organic frameworks (COFs), have only recently reached similar promising results as active materials for energy harvesting.[108,109] The encouraging thermoelectric performances of framework materials result from a high electrical conductivity combined with a very low thermal conductivity. The latter characteristic is mostly linked with a very low lattice thermal conductivity contribution: the phonons are unable to propagate across the vacant pores and there is a high degree of phonon scattering.[92] Electrical charge transport properties of COFs are often excellent (mobilities exceeding 1 $cm^2\ V^{-1}\ s^{-1}$), but these values are generally derived from time-resolved microwave conductivity (TRMC) measurements.[110,111] However, this technique measures the mobility within the nanometer regime and thus tends to overestimate the macroscopic mobility by disregarding domain boundary and electrode contact effects. This ambiguity highlights the challenge of transferring the good microscopic transport properties to the macroscopic regime. It explains also why investigations into COFs for thermoelectric applications have so far mainly been based on theoretical studies.

Chumakov and co-workers used density functional theory (DFT) and Boltzmann transport theory in their studies of phthalocyanine (Pc)-based COFs.[112] Taking into account the layered packing from experimental XRD patterns, they compared COFs with phenylene- (Pc-COF) and benzothiadiazole-based (Pc-BTDA) linkers (see Figure 4) and investigated their three-dimensional thermoelectric properties. While the Ni-containing COFs are predicted to perform better than the metal-free COFs due to better charge transport in the stacking direction, the nature of the linker strongly affects the in-plane properties. NiPc-BTDA displays positive Seebeck coefficients in all three directions, whereas NiPc-COF displays negative in-plane Seebeck coefficients; overall NiPc-COF is

predicted to be the better thermoelectric material with a high *ZT* value in the in-plane direction. The important role of the metal in Pc-based COFs was highlighted in a follow-up study investigating Co-, Cu- and ZnPc-COF, which all pack in a slipped stacking arrangement rather than the eclipsed stacking seen for NiPc-COF.[113] The weakened π-stacking interactions in turn lead to anisotropic in-plane properties. Due to its in-plane properties, CoPc-COF is predicted to display the best thermoelectric performance within the series.

Taking a step back and considering firstly a COF monolayer and its electronic properties, Brédas and co-workers have investigated theoretically a series of 2D materials including the pyrene and porphyrin-based frameworks Pyr-COF, Por-COF and ZnPor-COF.[114] Calculating electronic and electronic-vibration couplings, excellent ambipolar charge transport properties are predicted for Pyr-COF. Por-COF and ZnPor-COF are different: they are unipolar p-type materials with charge carrier mobilities ranging from 66 $cm^2 V^{-1} s^{-1}$ to 94 $cm^2 V^{-1} s^{-1}$ for the three monolayer materials. In another theoretical study, Brédas and co-workers highlighted the importance of 2D lattice symmetry and the impact on electronic band structures.[115] They considered more complex architectures, based on four-armed vertices (pyrene and porphyrin isomers) and on three-armed vertices (1,3,5-substituted benzenes and various benzotrithiophene isomers). In agreement with the work detailed above, both Pyr-COF and ZnPor-COF with four-armed vertices have highly dispersive electronic bands near the Fermi energy, which allow for efficient charge transport. The three-armed benzotrithiophenes reveal a strong dependence on lattice symmetry. Indicative of localized charge carriers and poor charge transport, the C_3 symmetrical isomer has a 2D structure with flat electronic bands around the Fermi energy. Conversely, the asymmetric benzo[1,2-*b*:3,4-*b*':5,6-*d*'']trithiophene[116] has a 2D structure with reduced lattice symmetry and therefore more dispersive valence and conduction bands, which should favor efficient charge transport. Yang and co-workers investigated another fused thiophene-based vertex and its 2D network, namely the

four-armed tetrathienoanthracene.[117] Among the two isomers studied, PTTA has dispersive valence and conduction bands as well as a sharp density-of-states peak near the Fermi level; the latter feature has been predicted by Mahan and Sofo to lead to a superior thermoelectric material.[118] The calculated hole and electron mobilities for PTTA are on the order of 8-16 $cm^2 V^{-1} s^{-1}$ with peak power factors predicted to be 2178 $\mu W m^{-1} K^{-2}$ and 1509 $\mu W m^{-1} K^{-2}$ for p- and n-type, respectively. The optimum thermoelectric performance was predicted at doping concentrations of 3.7×10^{20} cm^{-3} and 5.7×10^{20} cm^{-3} with corresponding electrical conductivities of 567 S cm^{-1} and 389 S cm^{-1} for p- and n-type, respectively.

The low electrical conductivity of organic semiconductors necessitates doping as a mean to significantly increase the charge carrier concentration and thus the conductivity. A few studies have outlined similar scenarios for semiconducting organic frameworks. Jiang and co-workers used the fully π-conjugated framework sp^2c-COF constructed from all sp^2-hybridised carbons to investigate the impact of doping on electrical properties.[119] For a so-called AA-stacking structure with tightly stacked layers (3.58 Å interlayer spacing), ordered pyrene columnar arrays and 1D pores, the electrical conductivity increased by 12 orders of magnitude upon exposure to iodine vapor. Pristine and iodine-doped sp^2c-COF samples were pressed into cm-sized pellets. The doped sample had ohmic conduction and a conductivity of 7.1×10^{-4} S cm^{-1}, compared to the much lower conductivity of 6.1×10^{-16} S cm^{-1} reported for the pristine sample. Further computational studies of this system support a p-type doping mechanism. Triiodide are formed and occupy the 1D pores. They contribute to a relatively high anion conductivity, on par with the measured electrical conductivity.[120] The pristine sp^2c-COF is predicted to have low electron and hole mobilities owing to flat electronic bands near the Fermi level, but p-doping leads to a much enhanced predicted hole mobility of 86 $cm^2 V^{-1} s^{-1}$. Using a similar doping protocol with iodine vapor, a ZnPc-based COF showed a 1000-fold conductivity enhancement upon doping.[121] Interestingly, Hall effect

measurements revealed an increased hole mobility of 22 $cm^2\ V^{-1}\ s^{-1}$ upon doping which was ascribed to a reduction of detrimental scattering processes upon doping. Bein and co-workers took a slightly different approach. They created frameworks with a highly electron-rich and thus easily oxidizable Wurster-type compound as vertex and employed not only iodine as p-type dopant but also antimony pentachloride and 2,3,5,6-tetrafluoro-7,7,8,8-tetracyanoquinodimethane (F4TCNQ).[122] F4TCNQ affords superior electrical conductivities upon doping. With, in addition, an optimized benzodithiophene linker, the electrical conductivities approach 4×10^{-2} S cm^{-1}. Remarkably, comparing the electrical properties of pressed pellets and oriented thin films measured in the van der Pauw geometry reveals no significant differences between isotropic and anisotropic charge transport upon doping. The reported conductivity values are of 3.67×10^{-2} S cm^{-1} and 2.18×10^{-2} S cm^{-1} for pellet and film, respectively.

In 2017, Wang and colleagues used a fluorene-based imine-linked COF (FL-COF1, Figure 4) to carry out the first thermoelectric characterization of a purely organic framework material.[123] Limited by a moderate electrical conductivity upon doping with iodine ($\approx 10^{-4}$ S cm^{-1}), a power factor of 0.063 µW $m^{-1}\ K^{-2}$ at room temperature was obtained owing to a high Seebeck coefficient of 2450 µV K^{-1}. The stability and robustness of the framework was evidenced by retained thermoelectric properties after one-month storage under ambient conditions. The framework also withstands de-doping and subsequent re-doping without a significant drop in thermoelectric performance (see Figure 6c). With the markedly higher electrical conductivities reported for other COFs, there is clearly significant room for improvement as more organic framework materials will be brought forward for detailed thermoelectric studies.

C.3.1.b. Microporous structures based on HPCs

Another class of microporous PCPs, the hypercrosslinked polymer (HPC) has been recently investigated for TE applications.

A first example of a thermoelectric HPC has been reported in 2020 by Sadak and coworkers. It consists in a highly porous triazatruxene (TAT) based hypercrosslinked polymer (TATHPC, see Figure 4).[124] The polymer network has been synthesized by the knitting method through Friedel-Crafts crosslinking of TAT (a fully aromatic molecule with a planar C3 symmetry) with methylal as an external crosslinker. The obtained TATHPC ordered in stacks separated by 4.13 Å and showed a microporous structure (calculated pore size 1.7 nm).

Inspired by the work on fluorene-based COFs previously described, DFT and Boltzmann transport were applied to estimate the TE transport coefficients and the band structure of TATHPC. Theoretical values of Seebeck and *ZT* have been found at 70-80 μV K^{-1} and 0.3, respectively, at 300K along the x and y-axes (in-plane directions).

To summarize, the large body of work on MOFs and COFs clearly illustrates how porosity can be precisely engineered through chemical control.[45,125] As such, microporous structures can be designed easily to host a chemical dopant without affecting the polymer matrix structure. Given the volatility of many chemical dopants however, attention must be paid to ensure the doping stability at elevated temperatures.[126] Combined with the excellent charge carrier mobilities reported for microporous systems (albeit often from measurements across short length scales), there is a significant potential for thermoelectric applications with these materials. Nonetheless, at present too few detailed investigations into thermoelectric properties make it difficult to draw general trends, but several theoretical studies confirm the significant potential of both COFs and HPCs.

Moving from microporous COFs and HPCs to systems with significantly larger pore sizes opens up a wide range of new challenges and opportunities within the meso- and macro-porous structures.

3.3.1. Meso- and macro-porous structures

3.3.2.a. Meso- and macro-porous structures based on PEDOT:PSS

Poly(3,4-ethylenedioxythiophene):poly(styrenesulfonate) (PEDOT:PSS) is one of the mainly used conducting polymer that can be formed as a physical gel porous structure. PEDOT:PSS is water soluble, easily processable, mechanically flexible and possesses a relatively high electrical conductivity which makes it a good candidate for the design of PCPs.[21,127] PEDOT is a p-type polymer obtained by oxidative polymerization of ethylenedioxythiophene (EDOT) monomer in the presence of PSS polyanions.[128] The PSS has a dual role. It acts as a charge balancing counter-ion and it allows PEDOT segments to be dispersed into aqueous media. In commercial blends, PSS is in excess to allow a good dispersion in water, but it is insulating, which decreases drastically the electrical conductivity of PEDOT:PSS. Treatment by several polar solvents, acidic or reducing agents have been tested to increase PEDOT:PSS conductivity in thin films.[129] Such treatments can improve electrical conductivity by removing part of the PSS and modifying PEDOT:PSS structure.[129–131] The treatments can be transposed to bulk 3D networks to tune the structure and maintain a sufficient charge conductivity within the PCP.[132] Indeed, if the porous structure is well controlled, inter-chain interactions and crystalline order can be improved resulting in more conductive porous polymers.

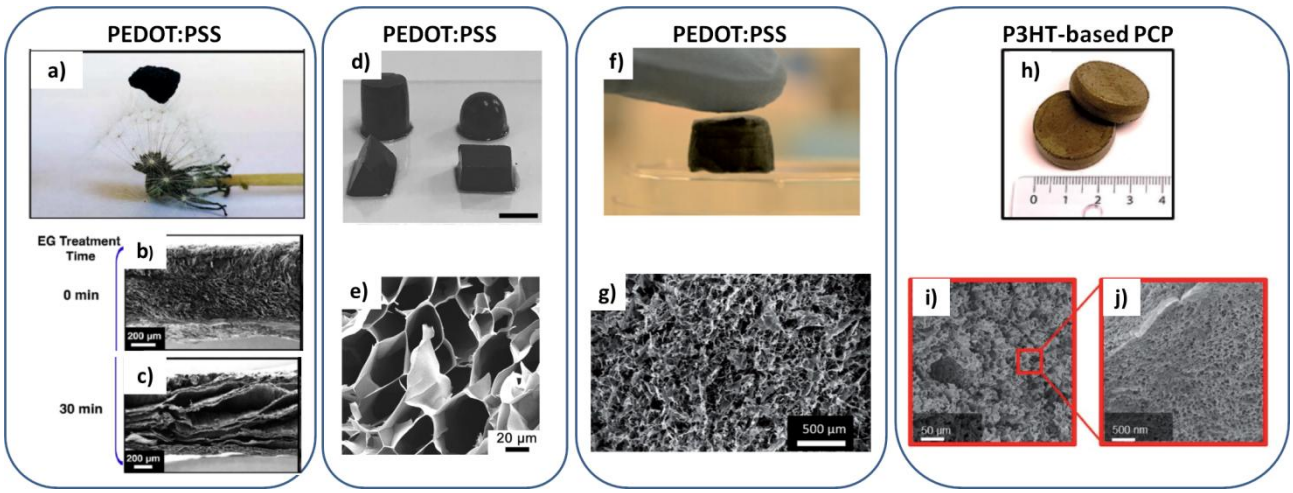

Figure 5 : Different PCP states and their macroporous structure observed by SEM. a - c) ultra-low density PEDOT:PSS cryogel placed on top of a dandelion and SEM characterizations of the gel before and after treatment with EG;[21] d – e) Digital pictures of PEDOT:PSS hydrogels with different geometric shapes (scale bars = 1 cm) and cross-section SEM image of a freeze- dried PEDOT:PSS hydrogel and after the treatment with concentrated H_2SO_4;[10] f - g) PEDOT:PSS, GOPS, and NFC PCP composite and SEM image of the internal structure;[25] h -j) P3HT "foam" and its internal porous structure characterized by SEM.[28] All panels have been reproduced with permission from J. APPL. POLYM. SCI. (a-c), Adv. Mater. (d-e), Adv. Funct. Mater. (f-g and h-j).

PEDOT:PSS hydrogels of interest for many applications, have been obtained via different processes: rehydration of thin films, ionic or dopant crosslinking, or in-situ oxidative polymerizations.[10,18,19,21,23,133] Only a few reports mention the use of those PEDOT:PSS hydrogels for TE applications. Interestingly, none of them apply the same process to fabricate the porous bulk materials. Hereafter, we report the various processes found in the literature.

Wang et al. use a direct flash-freeze technique with liquid N_2 of the PEDOT:PSS aqueous dispersion, which results in what is called in Table 1 "lyophilized PEDOT:PSS".[23] Polar solvents (such as ethylene glycol (EG) or N-methyl pyrrolidone (NMP)) were added to the polymer dispersion (5 %vol), prior to drying, promoting a structural change in PEDOT:PSS. These solvents are believed to remove the excessive insulating PSS from PEDOT domains and thus enhance the PEDOT domains crystallinity (decreased π-stacking distance and increase in crystalline domain size).[132,134] In this direct freeze-drying technique, the π-stacking interactions in PEDOT:PSS are strong enough and seem to promote the direct formation of a polymer network during ice sublimation process. The obtained 1 mm-thick samples are light and flexible. However, only a

couple of “voids” of 10-100 µm size can be observed within the polymer network by scanning electron microscopy (SEM).[23] The images do not really support a porous structure, unless the mean size of the pores is in the nanometer range, below the SEM resolution. Depending of the saturated vapor pressure of the solvent, smaller holes can be obtained which seem to impact positively the electrical conductivity (σ= 32 S cm^{-1} for EG treated sample as compared to 0.5 S cm^{-1} for non-treated sample). The authors further applied mechanical compression of the sample (decrease of the thickness from 1 to 0.1 mm and densification of the structure), which resulted in an interesting power factor of 1.24 µW m^{-1} K^{-2} (with σ= 35 S cm^{-1} and S = 18.8 µV K^{-1} for NMP treated sample, see Table 1). The in-plane thermal conductivity was 0.14 W m^{-1} K^{-1} (measured by transient hot wire technique) but the porosity of the sample was uncontrolled. For comparison, an in-plane thermal conductivity of 1.0 W m^{-1} K^{-1} has been measured by time domain thermoreflectance on a ~30 µm thick and dense PEDOT:PSS film ($\sigma \approx$ 500 S cm^{-1}).[135] This decrease of κ by an order of magnitude (accepting that the reported values are correct) highlights the positive effect of porosity on thermal insulation properties. Wang et al. further showed that such bulk thick samples can be integrated into TE generators made of six pairs of p-type PEDOT:PSS porous samples and n-type carbon nanotube fibers. The output performances are modest (maximum output power Pmax = 0.6 µW at ΔT = 68K), probably due to the poor control of the structure, but it represents the first demonstration of PCP integrated into a thermoelectric generator.

In a somewhat similar study, Maeda et al. prepared a porous PEDOT:PSS 3D network without using any crosslinker. However, gels were formed prior drying at ambient.[133] The PEDOT:PSS dispersion was deposited slowly at the bottom of a beaker filled by ethanol and then heated at 80°C for 20-150 min. Ethanol removes the excess of PSS from the PEDOT domains. A 3D network is formed by the PEDOT:PSS micelles interacting by van Der Waals or Hydrogen-bonds. Once physical gels are formed, they are left to dry at ambient air resulting in free-standing films with thicknesses ranging

from 1 to 30 µm (which we considered as xerogels). High electrical conductivities (300 to 1070 S cm^{-1}) were obtained depending on the sample thickness (21 µm to 1 µm, respectively). Interestingly, the Seebeck coefficient (16 -21 µV K^{-1}) is in the same range as for the flash-freeze dried samples, reported by Wang et al.[23] and for the typical value of PEDOT:PSS in thin films. No description of the microstructure is provided in this study. Drying the gel in air may result in some porosity. The porosity (and pore size) obtained by this method is probably smaller than the size of ice crystals (made during the freeze-drying process of the previously discussed method). Here, the porosity depends directly of the PEDOT:PSS gel morphology (although drying in air may lead to a denser film). A thinner and denser sample could explain the much higher electrical conductivities reported in Maeda's study.

Note that the PEDOT:PSS porous structure produced via freeze drying with no crosslinking agents are probably brittle, as mentioned by Khan et al.[26]

To overcome this possible weakness, Gordon and co-workers proposed to resort on ionic crosslinking to better control the network structure and the elasticity of both PEDOT:PSS hydrogels and cryogels.[21] In their approach, the free-standing thick films of PEDOT:PSS is first rehydrated. The resulting hydrogels are frozen in liquid N_2 and vacuum-pumped overnight. The method produces ultralight (d= 0.21- 0.25 mg cm^{-3}), robust, flexible and macroporous PEDOT:PSS samples (cryogels). Gordon and co-workers consider that the formation of this 3D structure is related to the ionically crosslinked polymeric hydrogel network formed when the thick PEDOT:PSS film is rehydrated. The pores of the dried matrix (thick film) are filled by water due to the hydrophilicity of the excess PSS. Their formation is induced by both ionic interactions between PEDOT and PSS, and hydrophilic/hydrophobic interactions between water and the polymer chains. This method provides bulk porous structure with pore size in the range of 50-100 µm according to SEM images of reference.[21] However, the porous network has a large-scale heterogeneity in its arrangement. In certain regions, the pores in the PCP network appear to preferentially align in the

same direction; the structure is denser at the interfaces, which may be due to local stronger capillary forces or structure collapse). These porous samples show limited charge conductivity - of a few S cm^{-1} only. To further improve their performance, the cryogels samples have been soaked in ethylene glycol for varying time (2-30 min). As previously mentioned, excess of PSS removal and use of polar solvent induce a polymer structural rearrangement and increased crystallinity. The treated EG cryogels treated in this way for long soaking time undergo such a morphological change, with thicker walls and a more layered-like structure (see Figure 5 b-c). This structure change increases σ to ~70 S cm^{-1} (after density correction). The Seebeck coefficient is slightly lower in the porous samples: on average at 16 µV K^{-1}. The power factor is thus ~1.8 µW m^{-1} K^{-2} (6 µW m^{-1} K^{-2} after density correction) for 500 µm thick cryogels (see Table 1). The thermal conductivity properties were not studied in this work.

The three pure PEDOT:PSS systems discussed above are amongst the few reports in the field of thermoelectricity. It is interesting to note that hydrogels of commercial PEDOT:PSS suspension can be easily produced in spite of their very low solid content (< 1.5 w% for PH1000). This polymer has indeed an extremely low critical concentration of gelation (CCG), about one order of magnitude lower than for more "conventional" polymers such as poly(vinyl alcohol) (PVA) (about 6 wt%).[136] Overall, the performances of the porous structures are lower than the films ones (see the values in Table 1 for PEDOT:PSS free standing film as comparison). However, as anticipated, porosity can minimize the thermal conduction and the Seebeck coefficient is marginally affected by the voids.

A better control over both the polymer chains order and the porous structure (during the gel formation and/or the gel drying process) should lead to higher charges conductivities. As a matter of fact, acid (or polar solvent) treatments of PEDOT:PSS hydrogels and dried scaffolds can lead to an increase of the pore wall thickness and a narrowing of pore sizes which can enhance the electrical conductivity. Yao et al.[10] have observed an increase in σ by a factor of 20 (from 0.46 to 8.8 S cm^{-1}) with a decrease of pore size by a factor 2 (80 down to 40 µm) after sulfuric acid post

treatment of their PEDOT:PSS cryogels (see the porous structure in Figure 5d-e). To limit a possible structure shrinkage during this post-drying step (secondary doping / solvent annealing) aiming at boosting the electrical conductivities, Yanagishima et al.[137] investigated a secondary doping of a PEDOT:PSS cryogel with methanol under supercritical condition ($ScCO_2$). Secondary doping by $ScCO_2$ methanol treatment or by dipping in DMSO leads to a remarkable enhancement of electrical conductivity (from 2 x 10^{-4} S cm^{-1} to 2 S cm^{-}, cf Figure 6a) due to the promotion of PEDOT crystallization. Note that the $ScCO_2$ treatment induces a more limited shrinkage than the dipping method.

Other techniques such as ice-templating[18,127,138] (similar to freeze-drying but with a control over the ice crystal growth) or microwave drying[139] could also be investigated to control the final porous structure. For instance, both the size and the unidirectional growth of the ice crystals during the freezing process of the hydrogels could leave behind highly ordered structures with potentially anisotropic TE properties. Please note that supercritical drying has not yet been investigated to directly produce aerogels for TE applications although this drying method is known to lead to very small pore size (~50 nm).[57]

The following part highlights the other strategy to overcome the apparent brittleness of PEDOT:PSS xero- and cryo-gels: the use of *polymer blends* in which PEDOT:PSS still plays the dual role of scaffolding and conducting material. Han,[25] Khan[26] and co-workers proposed to reinforce PEDOT:PSS dried gels by adding elastomeric cross-linkers such as glycidoxypropyl trimethoxysilane (GOPS) and a mechanical strengthener like nanofibrillated cellulose (NFC). The obtained PEDOT:PSS/GOPS/NCF cryogels are flexible and compressible (homogeneous porous structure of ~5O μm pore dimensions (see Figure 5f-g)). However, their electrical conductivities are limited to 10^{-3} S cm^{-1} because of the high amount of insulating part (NFC framework) in the sample.

There is definitely room for improvement and knowledge to gather in the field of PCPs for organic thermoelectrics. We would like to draw the attention of the readers on the possibility to consider hybrid structures (porous conductive polymer matrix blended with inorganic particles) to enhance the TE properties. As an example, Sun et al.[22] designed PEDOT:PSS cryogels blended with multi walls carbon nanotubes (MWCNT) and silver flakes (Ag). The resulting PEDOT:PSS/MWCNTS/Ag dried gels have a macroporous structure (pore size range: 10- 100 µm according to SEM pictures) with interconnected inorganic particles. The dense porous network is made of MWCNTs wrapped in PEDOT:PSS, showing a strong interaction between both the polymer matrix and the nanotubes, and Ag flakes that tend to agglomerate. The introduction of Ag flakes helps to reach higher electrical conductivity and Seebeck coefficient than for pure PEDOT:PSS cryogels (σ changing from 0.38 S cm^{-1} to 6.71 S cm^{-1} and *S* from 20 to 61.3 µV K^{-1} for 33.3 wt% of Ag). The real impact of the MWCNTs on the electrical conductivity could not be properly determined but wrapping of the MWCNTs with PEDOT:PSS allows a good phonons scattering and keeps a low thermal conductivity of the material between 0.06 to 0.11 W m^{-1} K^{-1}. *ZT* values reaching a maximum of 7.56 x 10^{-3} have been obtained.

Another example of composite has been described by Wang et al.[23] These authors fabricated PEDOT:PSS/Tellurium nanowires (Te-NWs) cryogels (following the previously described flash-frozen process) in order to increase the Seebeck coefficient of their porous materials. Typically, for inorganic materials such as Bi_2Te_3, the Seebeck coefficient is comprised between 150 and 200 µV K^{-1} for p-type materials[140] whereas for PEDOT:PSS it is around 15 to 20 µV K^{-1}. At high contents of Te-NWs, the Seebeck coefficient increased drastically (from 18.8 to 682 µV K^{-1}) but the electrical conductivity decreased from 35 to 0.002 S cm^{-1} (Figure 6e). The optimal power factor value was found at 30 wt% of Te-NWs and reaches 3.6 µW m^{-1} K^{-2}, three times higher than pure PEDOT:PSS dried gels. This improvement of the Seebeck coefficient may be explained by a potential energy barrier formed at the interface of PEDOT:PSS and Te-NWs filtering, which would allow only high-

energy charge carrier to pass through. This hypothesis rests on an intimate contact between the two phases, formation of an energy barrier at the interface of PEDOT:PSS and Te-NWs and finally a low nanomaterial content. A very promising *ZT* value of 2 x 10^{-2} has been reached within such composites after DMSO vapor treatment, demonstrating the importance of the structure control.

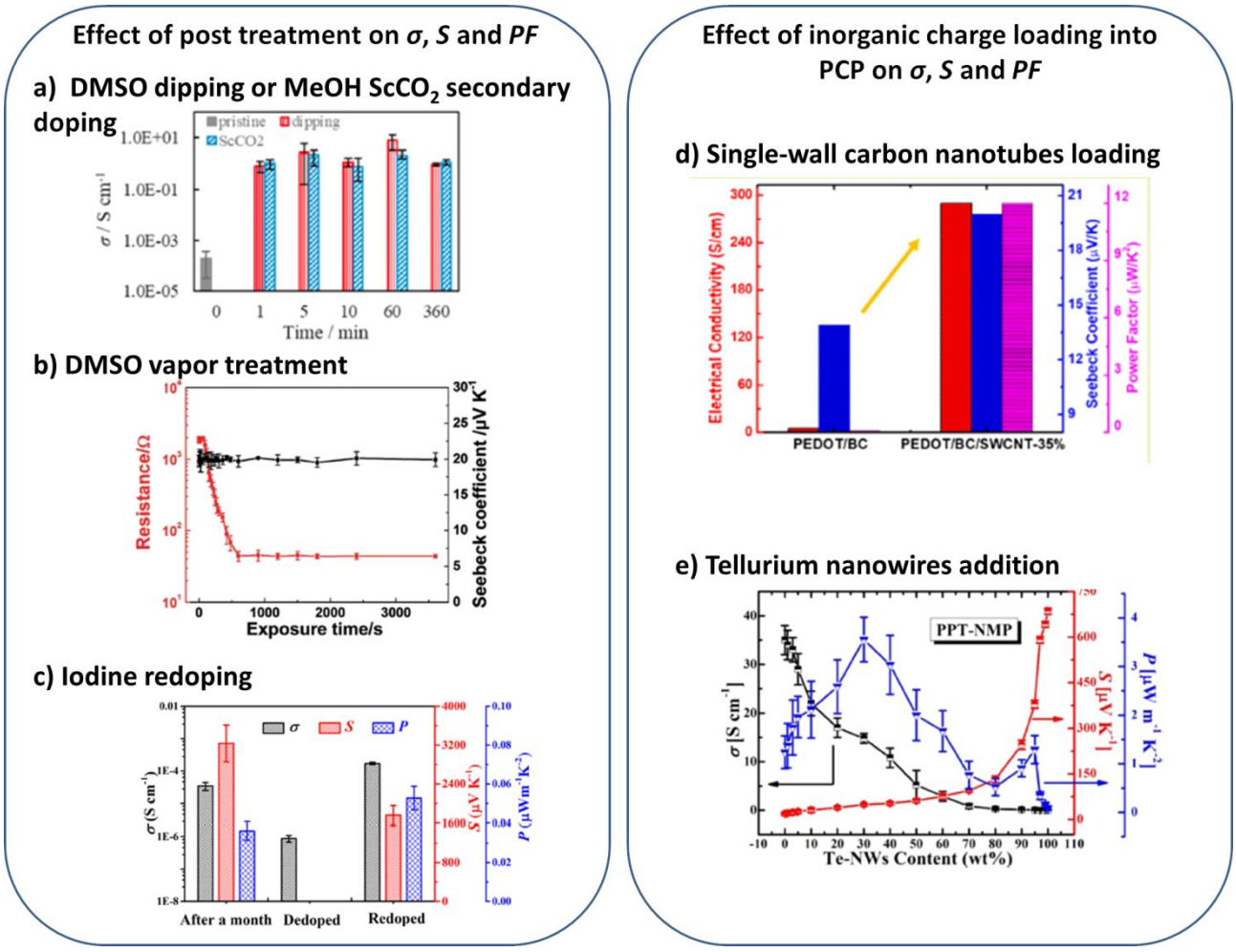

Figure 6: Some examples of PCP thermoelectric properties enhancement through post processing (a-c) or inorganic charge loading into the polymer matrix (d-f). All panels have been reproduced with permission from a) Polymer,[120] b) Adv. Funct. Mater.,[26] c) [109] and e) [25] ACS Appl. Mater. Interfaces, d) ACS Sustainable Chem. Eng.[18]

Finally, Jia et al. combined the structural benefit of bacterial cellulose (BC) fibers (low thermal conductivity in dried gel states due to a mesoporous network formation), with the high charge conductivities of single-walled carbon nanotube (SWNCTs) and PEDOT. In situ polymerization allowed PEDOT to be uniformly coated on BC nanofibers and SWNCTs. A flash-freeze drying of the dispersion provided ultralight PCP with a porosity up to 70%. The optimization of the structure, via mechanical pressing, together with an optimization of the SWNCTs loading afforded record PF of

12 μW m^{-1} K^{-2} in the porous bulk structure (Figure 6a). A thermal conductivity (calculated from the heat capacity and the bulk density of the sample) of 0.13 W m^{-1} K^{-1} was obtained. A TE prototype (assembled with 8 single legs of the porous composite) provided a maximum output power of 169 nW at ΔT = 65.6 K. This result reinforces the promising interest of PCP for TE application, especially for the heat conversion of small thermal gradient (in the microwatt to milliwatt power range) for which the conventional systems are inefficient.[64]

C.3.2.b. Meso- and macro-porous structures based on other conjugated polymers

Apart from the PEDOT based materials, other classes of investigated polymers for TE applications are based on chemically doped semi-conducting polymer films. A good control of their structure and an adequate tuning of their doping yield material properties comparable to the PEDOT based polymers. Is it possible however to fabricate porous bulk samples out of doped semi-conducting polymers to benefit from the high void structure and high surface area of PCPs?

Poly(3-hexylthiophene) (P3HT)[141,142] and poly(2,5-bis(3-alkylthiophene-2-yl)thieno[3,2-*b*]thiophene) (PBTTT)[143] can form gels via polymer fibers growth network, but little is known about their dried doped state. Kroon et al. were the first to design a millimeter-thick macroporous sample based on P3HT for TE application.[28] They used a thermally induced phase separation between P3HT and *ortho*-dichlorobenzene (o-DCB) upon cooling combined with a smart salt leaching approach. Small NaCl crystals (<20 μm) were used as porogens. The amount of salt directly impacts the final porosity of the sample. After liquid-liquid phase separation and solidification of the polymer sample, both *o*-DCB and NaCl salts were leached out by immersing the sample into methanol for some time. After drying in air, a P3HT "foam" was obtained with macropores of 14± 6 μm interconnected by mesopores of around 63 nm size, resulting in an estimated porosity of 66% (see Figure 5 h-j). This work illustrates the first fine control over the

porosity in a semi-conducting polymer although, as mentioned in the introduction, the porous sample does not strictly correspond to a foam, as no gas was involved in the preparation (but this terminology issue is of course of no consequence in the present context).

The authors further demonstrated that such a 3D porous structure facilitates the diffusion of dopant molecules (F4TCNQ in their specific case). Maximum values of 0.22 S cm^{-1} electrical conductivity and 68.4 μV K^{-1} Seebeck coefficient were obtained after doping the meso-/ macro-porous structure (see Table 1). Although the electrical conductivity has been decreased by an order of magnitude compared to the solid sample (σ= 3.24 S cm^{-1}), the Seebeck coefficient remains high in both doped structures (58.1 μV/K). The average thermal conductivity (in-plane and out-of-plane) for such 66% porous and 4 mm-thick sample was measured via the transient plane source method providing a value of 0.14 W m^{-1} K^{-1} (to be compared with the solid doped P3HT film: 0.32 W m^{-1} K^{-1}). The porous structure is beneficial in that it decreases the thermal conductivity and improves the doping efficiency (faster and more homogeneous through the entire thickness), but the decrease in electrical conductivity results in a lower *ZT* (2.3 x 10^{-4} for the foam, 1.0 x 10^{-3} for the thick solid sample). However, this study is a rare example that fully describes the structure and the TE properties of a new PCP. This process helps reach a controlled porous structure with pore size down to 63 nm. Further optimizations can be foreseen, such as the increase of charge carrier density (e.g. vapor phase doping of stronger oxidizing agent) and may lead to a higher electrical conductivity and enhanced performances.

Electrochemical synthesis is an alternative method to produce macroporous conducting polymer films of potential interest for TE applications. 10 μm-thick porous polyaniline (PANI) films have been produced via pulse electrodeposition in acidic solutions by Yang and co-workers.[144] The polymer nanofibers are formed in solution and are then deposited on a Ni plate forming an overlapped porous structure made of nanofibers. Fibers diameters and pore size can be controlled

by the pulse parameters, slightly impacting both electrical conductivity and Seebeck coefficient. Smaller fibers (~50 - 100 nm in diameter) and smaller pore size (~ 80 - 120 nm) result in the highest power factor (0.57 µW m^{-1} K^{-2}, as compared to 0.068 µW m^{-1} K^{-2} for 150-250 nm fiber diameters). The authors do demonstrate the positive impact of nanostructure on the thermoelectric properties, but the performances remain well below stretched PANI films doped with camphorsulfonic acid.[145] This electrochemical synthesis may possibly suffer from batch-to-batch reproducibility and the template working electrode may limit TE device fabrication.

Material	Material preparation	σ [S cm^{-1}]	S [µV K^{-1}]	PF [µW m^{-1} K^{-2}]	κ [W m^{-1} K^{-1}]	ZT at 298 K	Porosity/ structural information	Ref
PEDOT:PSS film	Free standing thick film treated with sulfuric acid	2500	20.6	107	In-plane: 0.64 Out-of-plane: 0.27	0.05 (in plane)	- Layered like structure - Few µm thick	146
Lyophilized PEDOT:PSS	Direct flash freezing of the dispersion containing polar solvent (no gelation prior drying) followed by mechanical compression	35	18.8	1.24	0.14 (in-plane)	2.6 x 10^{-3}	- No defined porosity, - Density: 0.25 g cm^{-3} - t= 100 µm after compression	23
PEDOT:PSS xerogel	Gel formation by weak interaction and removal of PSS excess – air drying	300	16	7.6	/	/	- Gel-film with no characterized microstructure - no mention nor control of porosity - t= 20 µm	133
PEDOT:PSS cryogel	Ionic crosslinking of PEDOT:PSS with EG – freeze drying and further EG soaking treatment	≈70	≈16	1.8	/	/	- Sheet like morphological arrays, 100 µm spaced and 20 µm thick walls. - t= 500 µm	21
Lyophilized PEDOT:PSS	Direct flash freezing of the dispersion and methanol post-treatment under 1h supercritical condition	2.23	17.9	0.072	0.032 (estimation based on porosity)	6.6 x 10^{-4}	- Density= 0.052 g cm^{-3} - Porosity 95.7 % - Sheet like morphological arrays ~1-20 µm spaced - t= 3-6 mm thick	137

Lyophilized PEDOT:PSS/ MWCNTS/Ag	Hybrid organic/inorganic aq. dispersion (33.3w% Ag load) - direct flash-freezing (no gelation process)	6.7	61.3	2.5	0.11	7.6×10^{-3}	- 3D macroporous network structure with MWCNTs wrapped in PEDOT:PSS - BET surface area =: 170 m^2 g - Pore size: 10 – 100 µm - t > mm thick	22
Lyophilized PEDOT:PSS/ Te NWs (30w%)	Direct flash freezing of the hybrid dispersion containing polar solvent (no gelation prior drying) followed by mechanical compression	15	49.2	3.6	0.16	6.7×10^{-3}	- Wrapped Te NWs in PEDOT:PSS - No well-defined porosity - Density: 0.25 g cm^{-3} - t= 100 µm after compression	23
Lyophilized PEDOT/SWCNT/Bacterial cellulose	Direct freeze drying of aq. dispersion of BC/SWCNT fibers coated with PEDOT. (best results given for 32wt % SWCNT). Films further pressed at 10 MPa)	291	20.3	12	0.13	2.8×10^{-2}	- SWCNT and BC 2D porous fiber network coated with PEDOT with coexistence of micro and mesopores (~ 20 nm) - Porosity ~ 70%. - BET surface area =28.04 m^2 g^{-1} - t= 169 µm (after compressing)	17
F4TCNQ doped P3HT "foam"	P3HT gelation by thermally induced phase separation followed by salt leaching and drying	0.22	68.4	0.1	0.14	2.3×10^{-4}	- Porosity 66%. - pores size: ~ 14 µm interconnected with smaller ones~ 63 nm - few mm thick macroporous sample	28
PANI porous films	Pulse potentiostatic electrochemical synthesis of PANI fibers in H2SO4	6.25	30.2	0.57	/	/	- "nanofibers overlapped structure - Pore size 80-120 nm - Fibers diameters (50-100 nm) - t= 10 µm thick	144
FL-COF1	Fluorene-based imine-linked COF doped with iodine	1×10^{-4}	2450	0.063	/	/	- Pore size 2.1 nm - BET surface area= 1308 m^2 g^{-1} before doping and 22 m^2 g^{-1} after doping	123

Table 1: Best reported values of thermoelectric properties (σ, S, PF, κ and ZT) from the different PCPs discussed herein. A reference PEDOT:PSS thin film has also been included for comparison. We have calculated ZT at 298K for a better comparison reading. BET stands for Brunauer-Emmett-Teller (BET) surface and gives an idea of the specific surface area (the larger value can be related to a larger number of smaller pores). t stands for sample thickness.

Table 1 shows that ZT is of comparable range of magnitude for the PEDOT:PSS reference in dense thin film and for the most efficient bulk PCPs. This is a very promising result as the decrease in thermal conductivity seems to compensate for the loss in electrical conductivity for thick and porous materials. Apart from FL-COF1, none of the reported results mentioned PCP with pore size inferior to the mean free path of air. There is therefore room for ZT improvement by tuning down the pore size and thus the thermal conductivity somehow independently of electrical conductivity. (Remark: a density normalized ZT value might be more appropriate to compare dense thin films and bulk PCP TE efficiencies).[28]

D. Further research avenues on PCPs as thermoelectrics

Figure 7 describes the important challenges and opportunities of PCPs as thermoelectrics.

To the best of our knowledge, research on porous organic materials for thermoelectrics has mainly focused on p-type materials but n-type PCPs are critically needed and should be developed in the near future. For instance, a couple of n-type COFs with promising electron mobilities have been reported in the literature.[111,147] Considering other kind of porous materials like MOFs, 2D coordination polymers (copper bis(dithiolene) complex (Cu-BHT)) have also shown very high electron mobility (116 $cm^2 V^{-1} s^{-1}$) and conductivity (1,580 $S cm^{-1}$).[148] Dried gels made from n-type polymers should also be feasible although their air stability is questionable, as for n-type semi-conducting polymers developed in thin films.

PIMs were included in our initial overview of porous organic materials. We note here that, to the best of our knowledge, they have not yet been investigated in the context of thermoelectrics. One possible limiting factor is their low electrical conductivity (because of the not fully conjugated

backbone and the twisted structure that hamper efficient chain packing). However, their microporous structure (of high interest for thermal conductivity, vide infra) could also host conducting fillers such as graphene or carbon nanotubes. We therefore anticipate that PIMs can become part of the field and develop alongside COFs, CMPs and HPCs as promising candidates for micro- and meso-porous hybrid thermoelectric materials.

Further opportunities exist for PCPs. Polymer blends could overcome the processability issue discussed above and enhance also the performances of the final material. As demonstrated by Zuo and co-authors, thin films of polymer blends with appropriate and complementary density of states are an efficient strategy to optimize the Seebeck coefficient.[72-73] A similar approach should also work for bulk porous materials. With a move to multi-component blends and composites, the parameter space increases exponentially. Although daunting, it highlights a huge potential for continued improvements in thermoelectric performance, thermal stability, mechanical strength and durability.

Further advances in processing are needed to fabricate samples in a reproducible fashion, both for insoluble crystalline materials like COFs and for very soft or brittle macroporous materials – namely foams and gels. Furthermore, bridging the gap in device fabrication from thin films to application relevant sample sizes is needed with increased understanding of structure-property relations across multiple length scales.

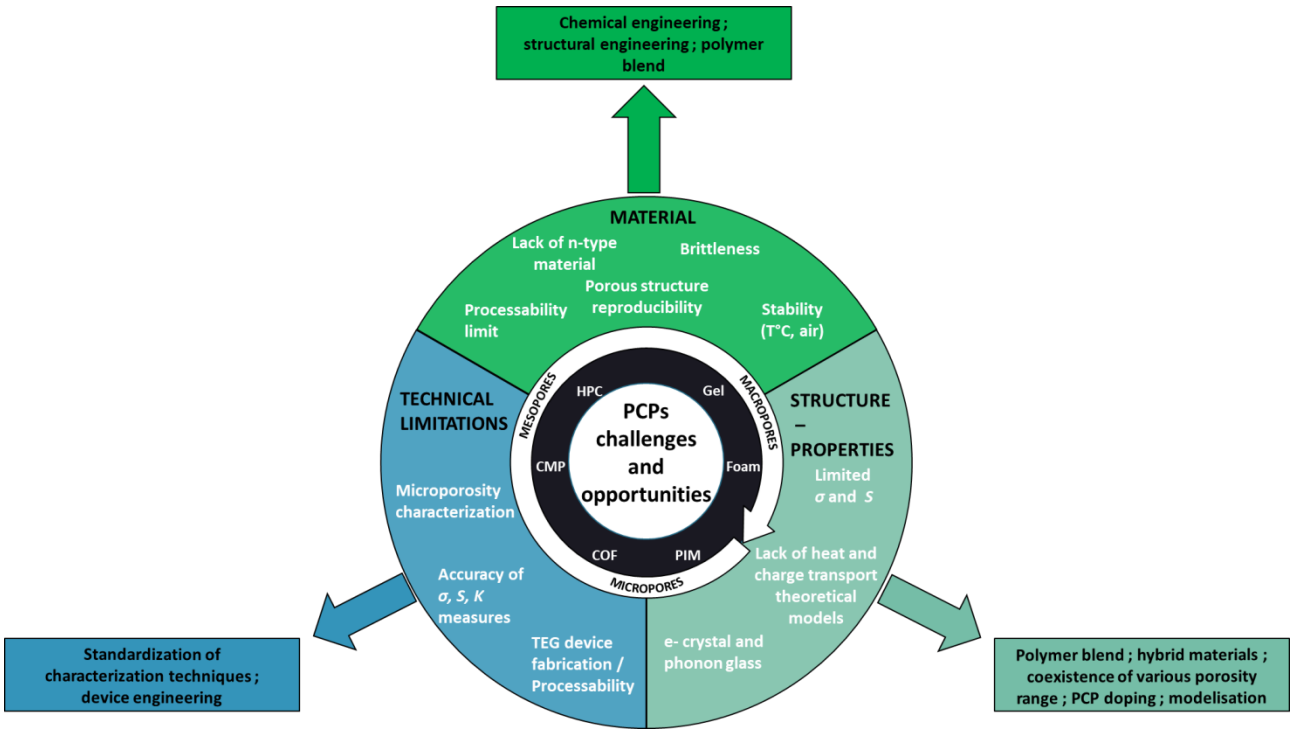

Figure 7: Challenges and opportunities of PCPs as efficient thermoelectric materials.

We have highlighted porous organic materials for their ability to diffuse easily dopant molecules into the open structure without disrupting electrically conducting pathways. In this context, it is important to also consider doping stability particular at elevated temperatures where these systems are expected to function. Molecular dopants are often relatively volatile small molecules and will as such be prone to diffuse both within and out of the porous material.[126,28] As such, further research are needed to develop a better understanding of doping stability in porous materials especially as a function of temperature. Note however that different synthesis strategies could also be considered, for example by covalently grafting the dopants[149] or by using self-doped polymers.[150]

Progresses on accuracy and standardization of TE properties measurements are still needed. Eventually, they will help establish clearer structure-properties relationships, which remain a prerequisite to achieve higher performances.

E. Summary and Perspective

Introduction of porosity, in a controlled fashion, into conducting polymers is emerging as new scientific and technologic concerns in thermoelectrics. In principle, porous PCPs can meet most of the requirements of an efficient thermoelectric material. Aside from their very low thermal conductivity, PCPs can host dopant molecules in their voids, therefore enhancing dopant diffusion into the bulk and improving charge carrier density. Both features are advantageous as compared to solid (dense) organic TE materials. The versatility of the synthetic chemistry toolbox allows for straightforward design of PCPs with a wide range of pore sizes and consequently with a high degree of tunability of the crucial electrical and thermal conductivities. This review has addressed the progresses made since 2015 in different synthesis and processing strategies to produce PCPs with a wide range of porosities (a few nanometers to hundreds of micrometers). The materials include COFs, HPCs, dried gels and porous films made of electro-polymerized fibers. Quite understandably, each material mentioned above has merits and limitations.

PCPs with designed and controlled microporous structures can be synthesized through elegant covalent chemistry. Issues with processability and structural control in the relevant length scales of device still limit the development of COFs and CMPs for thermoelectrics but theoretical studies and preliminary electrical data indicate that they are potentially high *ZT* materials.

Conducting polymer dried gels with meso- and/or macro-porous structure can be processed more easily. The control of the porous structure and the conducting polymer chain assemblies can be mastered during gelation, in the drying step or through post-processing treatment. Interestingly, coexistence of different ranges of pore sizes has been demonstrated within some gel based-PCPs. As a consequence, both phonon scattering and carrier transport were enhanced (mesopores) while limiting heat transport (macropores).

Given the wide range of pore sizes discussed herein, one obvious question is the ideal pore size for thermoelectric applications. On one hand, from a thermal transport perspective, significant lowering of the thermal conductivity is not achieved unless pore sizes are smaller than the mean free path of air molecules (<70 nm). On the other hand, the pores can also function as hosts (e.g. dopant molecules) which could enhance the charge carrier density. In such case, molecular design should include considerations such as pore size matching with dopants and the use of side chains that can interact non-covalently with dopants.[151]

The best experimental *ZT* efficiencies ($ZT > 2 \times 10^{-2}$) have been reported for macroporous hybrid materials. The origin of the improved efficiency is not yet fully understood, but the introduction of metal particles or carbon nanotubes into conducting polymer gels appears as a valuable and promising strategy to enhance the power factor of PCPs.

As the present time, only a few complete characterizations of PCPs have been described and general trends in structure-property relationships are difficult to establish in this emerging field. Continued efforts should be made both in overcoming technical issues in TE characterization of PCPs and in developing theoretical models of heat and charge transport in inhomogeneous porous structures. Accurate and reliable values of σ, S, and κ, are much needed to better compare TE parameters reported in different publications. They are also needed to validate the molecular and porous design concept aiming at improving the electrical charge transport or limiting the phonon propagation. Measuring protocols and practical guidelines are in need of standardization in order to avoid pitfalls and erroneous reports as it regrettably happened in the field of organic field effect transistors[152,153] and organic photovoltaics.[154]

To conclude, the routes to optimize *ZT,* the thermoelectric figure of merit, in PCPs, are wide and appealing to the vast multidisciplinary research community of (semi)-conducting polymers. This

review will stimulate hopefully interest in reaching a basic understanding of porous conducting polymer preparation and assist in their design to fulfil the requirements of thermoelectrics for low-temperature applications. Several material, technical and fundamental (structure-properties relationships) challenges need to be overcome. Systematic approaches are therefore required in the chemical, structural and device engineering of thermoelectric based PCPs.

Ultimately, achieving well-structured PCPs will push forward the development of other emerging organic electronic applications such as solar steam generator, solar thermoelectrics or triboelectric generator.

Author Contributions

All authors have contributed to the review work and manuscript writing.

Conflict of Interest

There are no conflicts to declare.

Acknowledgments

Bernard Lotz is gratefully acknowledged for his careful reading of the manuscript and pedagogical support. We thank Wiebke Drenckhan for the discussion on foams. Q. W. and L. B. acknowledge financial support by ANR JCJC 2019 (BODYTEG) and Région Grand Est 2020.

Keywords

Porous conducting polymer, organic thermoelectric, covalent organic framework, conducting gel, thermal conductivity

References

1 P. M. Budd and N. B. McKeown, *Polym. Chem.*, 2010, **1**, 63–68.

2 M. Noroozi, M. Panahi-Sarmad, M. Abrisham, A. Amirkiai, N. Asghari, H. Golbaten-Mofrad, N. Karimpour-Motlagh, V. Goodarzi, A. R. Bahramian and B. Zahiri, *ACS Appl. Energy Mater.*, 2019, **2**, 5319–5349.

3 Q. Sun, Z. Dai, X. Meng and F. S. Xiao, *Chem. Soc. Rev.*, 2015, **44**, 6018–6034.

4 J. R. Li, R. J. Kuppler and H. C. Zhou, *Chem. Soc. Rev.*, 2009, **38**, 1477–1504.

5 H. Zhang, Y. Zhang, C. Gu and Y. Ma, *Adv. Energy Mater.*, 2015, **5**, 1402175.

6 S. Chai, N. Hu, Y. Han, X. Zhang, Z. Yang, L. Wei, L. Wang and H. Wei, *RSC Adv.*, 2016, **6**, 49425–49428.

7 J. S. M. Lee, T. H. Wu, B. M. Alston, M. E. Briggs, T. Hasell, C. C. Hu and A. I. Cooper, *J. Mater. Chem. A*, 2016, **4**, 7665–7673.

8 H. Wang, D. Liu and P. Liu, *Microporous Mesoporous Mater.*, 2019, **284**, 141–150.

9 C.-C. Shih, Y.-C. Lin, M. Gao, M. Wu, H.-C. Hsieh, N.-L. Wu and W.-C. Chen, *J. Power Sources*, 2019, **426**, 205–215.

10 B. Yao, H. Wang, Q. Zhou, M. Wu, M. Zhang, C. Li and G. Shi, *Adv. Mater.*, 2017, **29**, 1–7.

11 H. Zhuo, Y. Hu, Z. Chen and L. Zhong, *Carbohydr. Polym.*, 2019, **215**, 322–329.

12 Y. Liao, H. Wang, M. Zhu and A. Thomas, *Adv. Mater.*, 2018, **30**, 1705710.

13 C. Zhang, Y. He, P. Mu, X. Wang, Q. He, Y. Chen, J. Zeng, F. Wang, Y. Xu and J. X. Jiang, *Adv. Funct. Mater.*, 2018, **28**, 1705432.

14 Q. Zhang, Q. Dai, M. Li, X. Wang and A. Li, *J. Mater. Chem. A*, 2016, **4**, 19132–19139.

15 X. Liu, J. Zhang, C. Zheng, J. Xue, T. Huang, Y. Yin, Y. Qin, K. Jiao, Q. Du and M. D. Guiver, *Energy Environ. Sci*, 2020, **13**, 297.

16 L. Cheng, X. Du, Y. Jiang and A. Vlad, *Nano Energy*, 2017, **41**, 193–200.

17 F. Jia, R. Wu, C. Liu, J. Lan, Y. H. Lin and X. Yang, *ACS Sustain. Chem. Eng.*, 2019, **7**, 12591–12600.

18 A. G. Guex, J. L. Puetzer, A. Armgarth, E. Littmann, E. Stavrinidou, E. P. Giannelis, G. G. Malliaras and M. M. Stevens, *Acta Biomater.*, 2017, **62**, 91–101.

19 A. M. D. Wan, S. Inal, T. Williams, K. Wang, P. Leleux, L. Estevez, E. P. Giannelis, C. Fischbach, G. G. Malliaras and D. Gourdon, *J. Mater. Chem. B*, 2015, **3**, 5040–5048.

20 N. Alegret, A. Dominguez-Alfaro and D. Mecerreyes, *Biomacromolecules*, 2019, **20**, 73–89.

21 J. J. U. Madeleine P. Gordon, Edmond W. Zaia, Preston Zhou, Boris Russ Nelson E. Coates, Ayaskanta Sahu, *J. Appl. Polym. Sci.*, 2017, **134**, 44070.

22 X. Sun, Y. Wei, J. Li, J. Zhao, L. Zhao and Q. Li, *Sci. China Mater.*, 2017, **60**, 159–166.

23 X. Wang, P. Liu, Q. Jiang, W. Zhou, J. Xu, J. Liu, Y. Jia, X. Duan, Y. Liu, Y. Du and F. Jiang, *ACS Appl. Mater. Interfaces*, 2019, **11**, 2408–2417.

24 Y. Wang, B. Yao, H. Chen, H. Wang, C. Li and Z. Yang, *Eur. Polym. J.*, 2019, **112**, 487–492.

25 S. Han, F. Jiao, Z. U. Khan, J. Edberg, S. Fabiano and X. Crispin, *Adv. Funct. Mater.*, 2017, **27**, 1–7.

26 Z. U. Khan, J. Edberg, M. M. Hamedi, R. Gabrielsson, H. Granberg, L. Wågberg, I. Engquist, M. Berggren and X. Crispin, *Adv. Mater.*, 2016, **28**, 4556–4562.

27 B. Lu, H. Yuk, S. Lin, N. Jian, K. Qu, J. Xu and X. Zhao, *Nat. Commun.*, 2019, **10**, 1043.

28 R. Kroon, J. D. Ryan, D. Kiefer, L. Yu, J. Hynynen, E. Olsson and C. Müller, *Adv. Funct. Mater.*, 2017, **27**, 1–8.

29 Y. Ko, J. Kim, D. Kim, G. Kwon, Y. Yamauchi and J. You, *Nanomaterials*, 2019, **9**, 612.

30 C. Gu, N. Huang, Y. Chen, L. Qin, H. Xu, S. Zhang, F. Li, Y. Ma and D. Jiang, *Angew. Chemie - Int. Ed.*, 2015, **54**, 13594–13598.

31 H. Bildirir, V. G. Gregoriou, A. Avgeropoulos, U. Scherf and C. L. Chochos, *Mater. Horizons*, 2017, **4**, 546–556.

32 S. Han, T. P. Ruoko, J. Gladisch, J. Erlandsson, L. Wågberg, X. Crispin and S. Fabiano, *Adv. Sustain. Syst.*, 2020, **4**, 2000004.

33 B. Lüssem, C. M. Keum, D. Kasemann, B. Naab, Z. Bao and K. Leo, *Chem. Rev.*, 2016, **116**, 13714–13751.

34 *IUPAC. Compendium of Chemical Terminology, 2nd ed. (the 'Gold Book'). Compiled by A. D. McNaught and A. Wilkinson. Blackwell Scientific Publications, Oxford*, 1997.

35 F. Vilela, K. Zhang and M. Antonietti, *Energy Environ. Sci.*, 2012, **5**, 7819–7832.

36 X. Li, C. Zhang, S. Cai, X. Lei, V. Altoe, F. Hong, J. J. Urban, J. Ciston, E. M. Chan and Y. Liu, *Nat. Commun.*, 2018, **9**, 1–8.

37 S. Liu, P. Gordiichuk, Z. S. Wu, Z. Liu, W. Wei, M. Wagner, N. Mohamed-Noriega, D. Wu, Y. Mai, A. Herrmann, K. Müllen and X. Feng, *Nat. Commun.*, 2015, **6**, 1–9.

38 Y. Wang, Y. Shi, L. Pan, Y. Ding, Y. Zhao, Y. Li, Y. Shi and G. Yu, *Nano Lett.*, 2015, **15**, 7736–7741.

39 S. Wan, J. Guo, J. Kim, H. Ihee and D. Jiang, *Angew. Chemie Int. Ed.*, 2009, **48**, 5439–5442.

40 J. X. Jiang, F. Su, A. Trewin, C. D. Wood, N. L. Campbell, H. Niu, C. Dickinson, A. Y. Ganin, M. J. Rosseinsky, Y. Z. Khimyak and A. I. Cooper, *Angew. Chemie - Int. Ed.*, 2007, **46**, 8574–8578.

41 L. Pan, G. Yu, D. Zhai, H. R. Lee, W. Zhao, N. Liu, H. Wang, B. C. K. Tee, Y. Shi, Y. Cui and Z. Bao, *Proc. Natl. Acad. Sci. U. S. A.*, 2012, **109**, 9287–9292.

42 A. A. Talin, A. Centrone, A. C. Ford, M. E. Foster, V. Stavila, P. Haney, R. A. Kinney, V. Szalai, F. El Gabaly, H. P. Yoon, F. Léonard and M. D. Allendorf, *Science*, 2014, **343**, 66–69.

43 J. Germain, J. M. J. Fréchet and F. Svec, *J. Mater. Chem.*, 2007, **17**, 4989–4997.

44 L. Heng, X. Wang, J. Zhai, Z. Sun and L. Jiang, *ChemPhysChem*, 2008, **9**, 1559–1563.

45 X. Chen, K. Geng, R. Liu, K. T. Tan, Y. Gong, Z. Li, S. Tao, Q. Jiang and D. Jiang, *Angew. Chemie Int. Ed.*, 2020, **59**, 5050–5091.

46 H. S. Sasmal, A. Halder, S. H. Kunjattu, K. Dey, A. Nadol, T. G. Ajithkumar, P. Ravindra Bedadur and R. Banerjee, *J. Am. Chem. Soc.*, 2019, **141**, 20371–20379.

47 D. W. Burke, C. Sun, I. Castano, N. C. Flanders, A. M. Evans, E. Vitaku, D. C. McLeod, R. H. Lambeth, L. X. Chen, N. C. Gianneschi and W. R. Dichtel, *Angew. Chemie Int. Ed.*, 2020, **59**, 5165–5171.

48 S. Wan, J. Guo, J. Kim, H. Ihee and D. Jiang, *Angew. Chemie - Int. Ed.*, 2008, **47**, 8826–8830.

49 X. Feng, X. Ding and D. Jiang, *Chem. Soc. Rev.*, 2012, **41**, 6010–6022.

50 J. S. M. Lee and A. I. Cooper, *Chem. Rev.*, 2020, **120**, 2171–2214.

51 C. Daniel, C. Dammer and J. M. Guenet, *Polymer*, 1994, **35**, 4243–4246.

52 Y. Shi and G. Yu, *Chem. Mater.*, 2016, **28**, 2466–2477.

53 W. He and X. Zhang, in *Conducting Polymers*, ed. F. Yilmaz, InTech, 2016, vol. i, pp. 49–72.

54 J.-M. Guenet, *Organogels : Thermodynamics, Structure, Solvent Role, and Properties*, Springer, New York, SpringerBr., 2016.

55 R. G. Weiss, *Molecular Gels*, Royal Society of Chemistry, Cambridge, 2018.

56 M. E. El-Naggar, S. I. Othman, A. A. Allam and O. M. Morsy, *Int. J. Biol. Macromol.*, 2020, **145**, 1115–1128.

57 X. Zhang, D. Chang, J. Liu and Y. Luo, *J. Mater. Chem.*, 2010, **20**, 5080–5085.

58 L. D. Zhao, S. H. Lo, Y. Zhang, H. Sun, G. Tan, C. Uher, C. Wolverton, V. P. Dravid and M. G. Kanatzidis, *Nature*, 2014, **508**, 373–377.

59 M. R. Burton, T. Liu, J. McGettrick, S. Mehraban, J. Baker, A. Pockett, T. Watson, O. Fenwick and M. J. Carnie, *Adv. Mater.*, 2018, **30**, 1801357.

60 J. Zhang, T. Zhang, H. Zhang, Z. Wang, C. Li, Z. Wang, K. Li, X. Huang, M. Chen, Z. Chen, Z. Tian, H. Chen, L. D. Zhao and L. Wei, *Adv. Mater.*, 2020, **32**, 2002702.

61 T. C. Harman, M. P. Walsh, B. E. Laforge and G. W. Turner, in *Journal of Electronic Materials*, Springer New York LLC, 2005, vol. 34, pp. L19–L22.

62 M. Campoy-Quiles, *Philos. Trans. R. Soc. A,* 2019, **377**, 20180352.

63 C. J. Yao, H. L. Zhang and Q. Zhang, *Polymers*, 2019, **11**, 107.

64 M. Goel and M. Thelakkat, *Macromolecules*, 2020, **53**, 36-32-3642.

65 O. Bubnova, Z. U. Khan, A. Malti, S. Braun, M. Fahlman, M. Berggren and X. Crispin, *Nat. Mater.*, 2011, **10**, 429–433.

66 D. Kiefer, R. Kroon, A. I. Hofmann, H. Sun, X. Liu, A. Giovannitti, D. Stegerer, A. Cano, J. Hynynen, L. Yu, Y. Zhang, D. Nai, T. F. Harrelson, M. Sommer, A. J. Moulé, M. Kemerink, S. R. Marder, I. Mcculloch, M. Fahlman, S. Fabiano and C. Müller, *Nat. Mater.*, 2019, **18**, 149-155.

67 A. M. Glaudell, J. E. Cochran, S. N. Patel and M. L. Chabinyc, *Adv. Energy Mater.*, 2015, **5**, 1401072.

68 M. N. Gueye, A. Carella, N. Massonnet, E. Yvenou, S. Brenet, J. Faure-Vincent, S. Pouget, F. Rieutord, H. Okuno, A. Benayad, R. Demadrille and J. P. Simonato, *Chem. Mater.*, 2016, **28**, 3462–3468.

69 A. Hamidi-Sakr, L. Biniek, J. L. Bantignies, D. Maurin, L. Herrmann, N. Leclerc, P. Lévêque, V. Vijayakumar, N. Zimmermann and M. Brinkmann, *Adv. Funct. Mater.*, 2017, **27**, 170017.

70 D. T. Scholes, P. Y. Yee, J. R. Lindemuth, H. Kang, J. Onorato, R. Ghosh, C. K. Luscombe, F. C. Spano, S. H. Tolbert and B. J. Schwartz, *Adv. Funct. Mater.*, 2017, **27**, 1702654.

71 S. N. Patel, A. M. Glaudell, K. A. Peterson, E. M. Thomas, K. A. O'Hara, E. Lim and M. L. Chabinyc, *Sci. Adv.*, 2017, **3**, e1700434.

72 G. Zuo, H. Abdalla and M. Kemerink, *Adv. Electron. Mater.*, 2019, **5**, 1800821. DOI:10.1002/aelm.201800821.

73 A. Abtahi, S. Johnson, S. M. Park, X. Luo, Z. Liang, J. Mei and K. R. Graham, *J. Mater. Chem. A*, 2019, **7**, 19774–19785.

74 S. Dongmin Kang and G. Jeffrey Snyder, *Nat. Mater.*, 2017, **16**, 252–257.

75 V. Vijayakumar, Y. Zhong, V. Untilova, M. Bahri, L. Herrmann, L. Biniek, N. Leclerc and M. Brinkmann, *Adv. Energy Mater.*, 2019, **9**, 1–12.

76 S. Lee, S. Kim, A. Pathak, A. Tripathi, T. Qiao, Y. Lee, H. Lee and H. Y. Woo, *Macromol. Res.*, 2020, 28, 531–552.

77 R. Kroon, D. A. Mengistie, D. Kiefer, J. Hynynen, J. D. Ryan, L. Yu and C. Müller, *Chem. Soc. Rev.*, 2016, **45**, 6147–6164.

78 O. Bubnova and X. Crispin, *Energy Environ. Sci.*, 2012, **5**, 9345–9362.

79 L. M. Cowen, J. Atoyo, M. J. Carnie, D. Baran and B. C. Schroeder, *ECS J. Solid State Sci. Technol.*, 2017, **6**, N3080–N3088.

80 L. Stepien, A. Roch, R. Tkachov and T. Gedrange, in Thermoelectrics for Power Generation - A look at trends in the Technology, eds. S. Skipidarov and M. Nikitin, Intechopen, 2016, pp. 47-69.

81 N. Hüsing and U. Schubert, *Angew. Chemie - Int. Ed.*, 2007, **37**, 22–45.

82 D. S. Smith, A. Alzina, J. Bourret, B. Nait-Ali, F. Pennec, N. Tessier-Doyen, K. Otsu, H. Matsubara, P. Elser and U. T. Gonzenbach, *J. Mater. Res.*, 2013, **28**, 2260–2272.

83 V. Apostolopoulou-Kalkavoura, P. Munier and L. Bergström, *Adv. Mater.*, 2020, **2001839**, 1–17.

84 J. (Jochen) Fricke, in *Springer proceedings in Physics*, 1986, pp. 94–103.

85 X. Lu, R. Caps, J. Fricke, C. T. Alviso and R. W. Pekala, *J. Non. Cryst. Solids*, 1995, **188**, 226–234.

86 C. Bi, G. H. Tang and W. Q. Tao, *J. Non. Cryst. Solids*, 2012, **358**, 3124–3128.

87 P. Levitz, *J. Phys. Chem.*, 1993, **97**, 3813–3818.

88 C. Bi, G. H. Tang, Z. J. Hu, H. L. Yang and J. N. Li, *Int. J. Heat Mass Transf.*, 2014, **79**, 126–136.

89 C. Bi and G. H. Tang, *Int. J. Heat Mass Transf.*, 2013, **64**, 452–456.

90 A. Henry, *Annu. Rev. Heat Transf.*, 2013, **17**, 485–520.

91 D. Scheunemann and M. Kemerink, *Phys. Rev. B*, 2020, **101**, 07520.

92 L. Sun, B. Liao, D. Sheberla, D. Kraemer, J. Zhou, E. A. Stach, D. Zakharov, V. Stavila, A. A. Talin, Y. Ge, M. D. Allendorf, G. Chen, F. Léonard and M. Dincă, *Joule*, 2017, **1**, 168–177.

93 H. Wang, W. Chu and G. Chen, *Adv. Electron. Mater.*, 2019, 5, 1900167.

94 K. Walzer, B. Männig, M. Pfeiffer and K. Leo, *Chem. Rev.*, 2007, **107**, 1233–1271.

95 R. Noriega, J. Rivnay, K. Vandewal, F. P. V. Koch, N. Stingelin, P. Smith, M. F. Toney and A. Salleo, *Nat. Mater.*, 2013, **12**, 1038–1044.

96 M. C. J. M. Vissenberg and M. Matters, *Phys. Rev. B*, 1998, **57**, 12964–12967.

97 H. Bässler and A. Köhler, *Top. Curr. Chem.*, 2012, **312**, 1–65.

98 Y. K. Lan and C. I. Huang, *J. Phys. Chem. B*, 2009, **113**, 14555–14564.

99 X. Zhang, H. Bronstein, A. J. Kronemeijer, J. Smith, Y. Kim, R. J. Kline, L. J. Richter, T. D. Anthopoulos, H. Sirringhaus, K. Song, M. Heeney, W. Zhang, I. McCulloch and D. M. Delongchamp, *Nat. Commun.*, 2013, **4**, 1–9.

100 R. J. Kline and M. D. McGehee, *Polym. Rev.*, 2006, **46**, 27–45.

101 N. F. Mott and E. A. Davis, *Electronic processes in non-crystalline materials*, Oxford Cla., 1979.

102 N. F. Mott, *J. Phys. C Solid State Phys.*, 1987, **20**, 3075–3102.

103 S. L. Suib, *J. Mater. Chem.*, 2008, **18**, 1623–1631.

104 R. Goodall, L. Weber and A. Mortensen, *J. Appl. Phys.*, 2006, **100**, 44912.

105 P. S. Liu, T. F. Li and C. Fu, *Mater. Sci. Eng. A*, 1999, **268**, 208–215.

106 H. Topsøe, *Bridg. Technol.*, 1968.

107 K. J. Erickson, F. Léonard, V. Stavila, M. E. Foster, C. D. Spataru, R. E. Jones, B. M. Foley, P. E. Hopkins, M. D. Allendorf and A. A. Talin, *Adv. Mater.*, 2015, **27**, 3453–3459.

108 M. Dogru and T. Bein, *Chem. Commun.*, 2014, **50**, 5531–5546.

109 Y. Yusran, Q. Fang and V. Valtchev, *Adv. Mater.*, 2020, **32**, 2002038.

110 S. Wan, F. Gándara, A. Asano, H. Furukawa, A. Saeki, S. K. Dey, L. Liao, M. W. Ambrogio, Y. Y. Botros, X. Duan, S. Seki, J. F. Stoddart and O. M. Yaghi, *Chem. Mater.*, 2011, **23**, 4094–4097.

111 X. Ding, L. Chen, Y. Honsho, X. Feng, O. Saengsawang, J. Guo, A. Saeki, S. Seki, S. Irle, S. Nagase, V. Parasuk and D. Jiang, *J. Am. Chem. Soc.*, 2011, **133**, 14510–14513.

112 Y. Chumakov, F. Aksakal, A. Dimoglo, A. Ata and S. A. Palomares-Sánchez, *J. Electron. Mater.*, 2016, **45**, 3445–3452.

113 Y. Chumakov and G. Bayram, *J. Electron. Mater.*, 2020, **49**, 5498–5507.

114 S. Thomas, H. Li, R. R. Dasari, A. M. Evans, I. Castano, T. G. Allen, O. G. Reid, G. Rumbles, W. R. Dichtel, N. C. Gianneschi, S. R. Marder, V. Coropceanu and J. L. Brédas, *Mater. Horizons*, 2019, **6**, 1868–1876.

115 S. Thomas, H. Li, C. Zhong, M. Matsumoto, W. R. Dichtel and J. L. Bredas, *Chem. Mater.*, 2019, 31, 3051–3065.

116 C. B. Nielsen, J. M. Fraser, B. C. Schroeder, J. Du, A. J. P. White, W. Zhang and I. McCulloch, *Org. Lett.*, 2011, **13**, 2414–2417.

117 T. Deng, X. Yong, W. Shi, Z. M. Wong, G. Wu, H. Pan, J. S. Wang and S. W. Yang, *J. Mater. Chem. A*, 2020, **8**, 4257–4262.

118 G. D. Mahan and J. O. Sofo, *Proc. Natl. Acad. Sci. U. S. A.*, 1996, **93**, 7436–7439.

119 E. Jin, M. Asada, Q. Xu, S. Dalapati, M. A. Addicoat, M. A. Brady, H. Xu, T. Nakamura, T. Heine, Q. Chen and D. Jiang, *Science*, 2017, **357**, 673–676.

120 Q. Zhang, M. Dai, H. Shao, Z. Tian, Y. Lin, L. Chen and X. C. Zeng, *ACS Appl. Mater. Interfaces*, 2018, **10**, 43595–43602.

121 M. Wang, M. Wang, H. H. Lin, M. Ballabio, H. Zhong, M. Bonn, S. Zhou, T. Heine, E. Cánovas, R. Dong and X. Feng, *J. Am. Chem. Soc.*, 2020, **142**, 21622–21627.

122 J. M. Rotter, R. Guntermann, M. Auth, A. Mähringer, A. Sperlich, V. Dyakonov, D. D. Medina and T. Bein, *Chem. Sci.*, 2020, **11**, 12843–12853.

123 L. Wang, B. Dong, R. Ge, F. Jiang and J. Xu, *ACS Appl. Mater. Interfaces*, 2017, **9**, 7108–7114.

124 A. E. Sadak, E. Karakuş, Y. M. Chumakov, N. A. Dogan and C. T. Yavuz, *ACS Appl. Energy Mater.*, 2020, **3**, 4983–4994.

125 J. Yang and Y. W. Yang, *Small*, 2020, **16**, 1–24.

126 K. Kang, S. Schott, D. Venkateshvaran, K. Broch, G. Schweicher, D. Harkin, C. Jellett, C. B. Nielsen, I. McCulloch and H. Sirringhaus, *Mater. Today Phys.*, 2019, **8**, 112–122.

127 X. Zhang, C. Li and Y. Luo, *Langmuir*, 2011, **27**, 1915–1923.

128 S. Kirchmeyer and K. Reuter, *J. Mater. Chem.*, 2005, **15**, 2077–2088.

129 Z. Zhu, C. Liu, F. Jiang, J. Xu and E. Liu, *Synth. Met.*, 2017, **225**, 31–40.

130 S. Zhang, P. Kumar, A. S. Nouas, L. Fontaine, H. Tang and F. Cicoira, *APL Mater.*, 2015, **3**, 014911.

131 T. R. Chou, S. H. Chen, Y. Te Chiang, Y. T. Lin and C. Y. Chao, *J. Mater. Chem. C*, 2015, **3**, 3760–3766.

132 J. Wang, K. Cai and S. Shen, *Org. Electron.*, 2014, **15**, 3087–3095.

133 R. Maeda, H. Kawakami, Y. Shinohara, I. Kanazawa and M. Mitsuishi, *Mater. Lett.*, 2019, **251**, 169–171.

134 C. M. Palumbiny, F. Liu, T. P. Russell, A. Hexemer, C. Wang and P. Müller-Buschbaum, *Adv. Mater.*, 2015, **27**, 3391–3397.

135 J. Liu, X. Wang, D. Li, N. E. Coates, R. A. Segalman and D. G. Cahill, *Macromolecules*, 2015, **48**, 585–591.

136 M. Liu, R. Cheng and R. Qian, *J. Polym. Sci. Part B Polym. Phys.*, 1995, **33**, 1731–1735.

137 N. Yanagishima, S. Kanehashi, H. Saito, K. Ogino and T. Shimomura, *Polymer*, 2020, **206**, 122912.

138 M. A. Shahbazi, M. Ghalkhani and H. Maleki, *Adv. Eng. Mater.*, 2020, 22, 2000033.

139 N. Tonanon, Y. Wareenin, A. Siyasukh, W. Tanthapanichakoon, H. Nishihara, S. R. Mukai and H. Tamon, *J. Non. Cryst. Solids*, 2006, **352**, 5683–5686.

140 H. J. Goldsmid, *Materials*, 2014, 7, 2577–2592.

141 G. M. Newbloom, K. M. Weigandt and D. C. Pozzo, *Macromolecules*, 2012, **45**, 3452–3462.

142 K. Samanta, J. M. Guenet and S. Malik, *Macromolecules*, 2019, **52**, 8569–8576.

143 H. L. Yi and C. C. Hua, *Soft Matter*, 2018, **14**, 1270–1280.

144 W. Yang, H. Xu, Y. Li and W. Wang, *J. Electron. Mater.*, 2017, **46**, 4815–4824.

145 H. Yan, T. Ohta and N. Toshima, *Macromol. Mater. Eng.*, 2001, **286**, 4815-4824.

146 Z. Li, H. Sun, C. L. Hsiao, Y. Yao, Y. Xiao, M. Shahi, Y. Jin, A. Cruce, X. Liu, Y. Jiang, W. Meng, F. Qin, T. Ederth, S. Fabiano, W. M. Chen, X. Lu, J. Birch, J. W. Brill, Y. Zhou, X. Crispin and F. Zhang, *Adv. Electron. Mater.*, 2018, **4**, 1–8.

147 X. Feng, L. Liu, Y. Honsho, A. Saeki, S. Seki, S. Irle, Y. Dong, A. Nagai and D. Jiang, *Angew. Chemie Int. Ed.*, 2012, **51**, 2618–2622.

148 X. Huang, P. Sheng, Z. Tu, F. Zhang, J. Wang, H. Geng, Y. Zou, C. A. Di, Y. Yi, Y. Sun, W. Xu and D. Zhu, *Nat. Commun.*, 2015, **6**, 1–8.

149 A. O. Patil, Y. Ikenoue, N. Basescu, N. Colaneri, J. Chen, F. Wudl and A. J. Heeger, *Synth. Met.*, 1987, **20**, 151–159.

150 C. K. Mai, R. A. Schlitz, G. M. Su, D. Spitzer, X. Wang, S. L. Fronk, D. G. Cahill, M. L. Chabinyc and G. C. Bazan, *J. Am. Chem. Soc.*, 2014, **136**, 13478–13481.

151 J. Liu, G. Ye, H. G. O. Potgieser, M. Koopmans, S. Sami, M. I. Nugraha, D. R. Villalva, H. Sun, J. Dong, X. Yang, X. Qiu, C. Yao, G. Portale, S. Fabiano, T. D. Anthopoulos, D. Baran, R. W. A. Havenith, R. C. Chiechi and L. J. A. Koster, *Adv. Mater.*, 2021, **33**, 2006694.

152 H. H. Choi, K. Cho, C. D. Frisbie, H. Sirringhaus and V. Podzorov, *Nat. Mater.*, 2017, 17, 2–7.

153 I. Mcculloch, A. Salleo and M. Chabinyc, *Science*, 2016, **352**, 1521–1522.

154 E. J. Luber and J. M. Buriak, *ACS Nano*, 2013, **7**, 4708–4714.

Table of content

Porous conducting polymers are intriguing heat harvester candidates. This review focuses on the different strategies to vary the porosity range (from micro- to macro- pores) and their impact on thermoelectric properties.

Porous conducting polymers for thermoelectrics